

One Dimensional Dynamical Models of the Carina Nebula Bubble

E. Harper-Clark¹ and N. Murray^{1,2}

h-clark@astro.utoronto.ca, murray@cita.utoronto.ca

ABSTRACT

We have tested the two main theoretical models of bubbles around massive star clusters, Castor et al. and Chevalier & Clegg, against observations of the well studied Carina Nebula. The Castor et al. theory over-predicts the X-ray luminosity in the Carina bubble by a factor of 60 and expands too rapidly, by a factor of 4; if the correct radius and age are used, the predicted X-ray luminosity is even larger. In contrast, the Chevalier & Clegg model under-predicts the X-ray luminosity by a factor of 10. We modify the Castor et al. theory to take into account lower stellar wind mass loss rates, radiation pressure, gravity, and escape of or energy loss from the hot shocked gas. We argue that energy is advected rather than radiated from the bubble. We undertake a parameter study for reduced stellar mass loss rates and for various leakage rates and are able to find viable models. The X-ray surface brightness in Carina is highest close to the bubble wall, which is consistent with conductive evaporation from cold clouds. The picture that emerges is one in which the hot gas pressure is far below that found by dividing the time-integrated wind luminosity by the bubble volume; rather, the pressure in the hot gas is set by pressure equilibrium with the photoionized gas at $T = 10^4$ K. It follows that the shocked stellar winds are not dynamically important in forming the bubbles.

Subject headings: ISM:bubbles

1. INTRODUCTION

Over a dynamical time only 2% of the gas in a typical disk galaxy is turned into stars (Kennicutt 1998), in spite of the fact that the disks are marginally gravitationally stable (Kennicutt 1989). This puzzling result suggests that something other than gravity plays

¹Canadian Institute for Theoretical Astrophysics, 60 St. George Street, University of Toronto, Toronto, ON M5S 3H8, Canada

²Canada Research Chair in Astrophysics

a (negative) role in star formation. Passive support against collapse and subsequent star formation can come from magnetic fields or turbulence. Examination of star forming galaxies and individual star forming regions commonly shows evidence for more active support against gravity, for example, expanding bubbles. Active mechanisms, which come under the rubric of ‘feedback’, include energy or momentum input by active galactic nuclei, or from stars. Since most disk galaxies, including our own Milky Way, show little or no nuclear activity, and since bubbles in individual star forming regions are clearly not due to active galactic nuclei, in this paper we focus on feedback from stars.

Stars of type B2 and earlier supply several types of feedback, including protostellar jets, main-sequence stellar winds, radiation pressure, gas pressure associated with ionizing radiation, and supernovae. The mechanical energy imparted via a supernova is comparable to that injected by the star’s stellar wind over its lifetime (Castor et al. 1975). However, it is clear that many observed bubbles have formed before any of the stars in the central cluster have exploded in a supernova. Since we are interested in bubble formation, we will ignore supernovae, leaving open the question of whether supernovae provide the feedback necessary to limit the rate of star formation.

There are two competing theoretical models of stellar wind bubbles in the literature: that of Castor et al. (i.e. Castor et al. (1975) and Weaver et al. (1977)) and that of Chevalier & Clegg (1985), as implemented in, e.g., Stevens & Hartwell (2003). In the theory explored by Castor, the stellar-wind shocked gas is confined by a cool shell of swept up interstellar medium (ISM). In contrast, the Chevalier & Clegg theory ignores any surrounding material and simply has a steady-state wind. The temperatures, pressures and predicted sizes of the X-ray emitting regions in the two theories are significantly different.

However, these differences can be masked if the stellar content of the bubble is not well constrained. Recent work by Smith (2006a) provides a detailed accounting of the number of early type stars in the well studied Carina nebula. Combined with the wealth of multi-wavelength observations available for Carina, this allows for a stringent test of the models.

Observations of star forming regions in the Milky Way show that the gas density is highly variable. In particular, the projected surface density is consistent with a log-normal distribution, e.g., Goodman, Pineda, & Schnee (2008); Wong et al. (2008). These observations are consistent with both analytic and numerical studies of supersonic turbulent flows, which predict log-normal density and column density distributions (Passot & Vazquez-Semadeni 1998; Ostriker Stone & Gammie 2001). These results call into question one of the fundamental assumptions of the Castor et al. model, that the gas surrounding the central star or star cluster has a rather uniform density distribution. If the mass distribution is non-uniform, the shell swept up by the shocked stellar wind is likely to have holes. If so, this will lead to incomplete confinement of the hot gas and a consequent reduction in the pressure and

associated X-ray emission of the hot gas. Such a situation would be intermediate between the Castor et al. model of a completely confined wind and the Chevalier & Clegg picture of a free-flowing wind. We explore such intermediate models below.

This paper is organized as follows. In the next section we summarize some relevant observations of Carina, as well as some order of magnitude estimates of the pressures and forces acting on the surrounding cold, dense gas. In §3 (and the appendices) we describe the Chevalier & Clegg model, the Castor et al. model, and our modifications to the Castor et al. models. We also describe our numerical methods. In §4 we present the results of our modeling, including a parameter study of the (modified) Castor et al. bubbles. In §5 we discuss the X-ray emission. In §6 we discuss the results and compare to previous work. We give our conclusions in the final section.

2. OBSERVATIONS OF CARINA

The distance to Carina is 2.3 kpc (Allen & Hillier 1993; Smith 2006b). The complex contains about 70 O stars (Smith 2006a), of which 47 (including evolved massive stars) reside in Trumpler 16 (Tr 16), a star cluster with a radius $r \sim 3$ pc. This makes Carina one of the most massive (and best studied) star formation regions in the Milky Way. The bolometric luminosity emerging from the stars is 9.6×10^{40} erg s⁻¹. This is about twice the far infrared luminosity of the complex (Smith & Brooks 2007a), indicating that half the stellar flux is intercepted by dust grains within $\sim 10 - 20$ pc of the stars.

We note that this rather low ratio of infrared to bolometric luminosity is consistent with the fact that we can see Tr 16 in the optical, and with turbulent models of the ISM, but it is inconsistent with the assumption of the Castor et al. model that the ISM and swept-up bubble shell surrounding the cluster is homogeneous. It suggests that hot gas can escape the bubble, a point we return to later.

The number of ionizing photons emitted per second is $Q = 9 \times 10^{50}$ s⁻¹. The kinetic energy of the stellar winds is $L_w \sim 3.5 \times 10^{38}$ erg s⁻¹, assuming standard estimates of the mass loss rates; we argue below that this is likely to be an overestimate by a factor of 3 – 10. The massive stars of Tr 16 are responsible for about 70% of the bolometric and stellar wind luminosity and of the ionizing flux of the entire nebula; see Table 1.

A reasonably reliable estimate for the age of Tr 16 is given by the age of η Carina, currently the most massive star in the region. η Carina is ~ 3.6 million years old, since it has clearly evolved off the main sequence, while estimates of its initial mass based on its current luminosity and stellar models (Bressan et al. 1993) are in the range of $120M_\odot$. We thus assume the cluster is approximately 3.6 million years old. It is believed that no supernovae

have occurred in Tr 16 (Retallack 1983; Lopez & Meaburn 1984; Whiteoak 1994), but in any case the integrated energy deposited by the winds, 4×10^{52} erg, substantially exceeds the energy input of a supernova, of order 10^{51} erg.

For the 17th anniversary of the Hubble Space Telescope, Smith & Brooks (2007b) took a 50 light-year-wide mosaic of the centre of the Carina nebula. This image has unprecedented detail of globules within the bubble and star birth at the edge of the bubble. Triggered star formation around the edge of the bubble in Carina is also observed in X-ray and Near-IR studies of Carina (Sanchawala et al 2007). There are many directional markers, such as pillars, showing that the bubble edge is dominated by the effects of Tr 16. The images show that the main bubble shell is markedly non-spherical. Smaller bubble structures within the main bubble can be seen. Smith & Brooks (2007a) compiled a multi-wavelength analysis of the Carina nebula enabling approximate edges to the bubble to be located. We estimate radii in the range 10 – 20 pc.

There have been many observations of Carina in X-rays, which establish the existence of diffuse emission from the nebula itself (Seward et al. 1979; Flaccomio 2005; Hamaguchi et al. 2007a,b). The largest area coverage of the Carina region is provided by Seward et al. (1979), who used the Einstein Observatory to find a diffuse X-ray emission of 4.8×10^{34} erg s⁻¹ for the 0.5 – 3.0 keV band (scaled from their distance estimate of 2.6 kpc to 2.3 kpc).

The pressure inside the bubble surrounding Tr 16 contributes directly to the outward force on the surrounding material. We estimate the pressure in several ways.

First, the pressure can be calculated from the free-free radio emission, e.g., as reported in Huchtmeier & Day (1975), who measured a flux of $S_\nu = 1.43 \times 10^3$ Jy. From calculations of the expected Bremsstrahlung radio flux at the observer

$$n_{HII} = 3.6 \left(\frac{R}{pc} \right)^{-3/2} \left(\frac{D}{kpc} \right) \left(\frac{T}{K} \right)^{1/4} \left(\frac{S_\nu}{Jy} \right)^{1/2} \epsilon_{HII}^{-1/2} \text{ cm}^{-3}, \quad (1)$$

where ϵ_{HII} is the volume filling factor of the H II gas inside the bubble. For the radius of the bubble, $R = 10$ pc and distance, $D = 2.3$ kpc, we find $n_{HII} = 100 \text{ cm}^{-3}$ for $T_{HII} = 10^4 \text{ K}$. Thus, $P = 1.4 \times 10^{-10} \epsilon_{HII}^{-1/2} \text{ dynes cm}^{-2}$.

As a consistency check, we note that pressure of an H II region powered by a cluster emitting Q ionizing photons per second is given by

$$P_{HII} = \sqrt{\frac{3Q}{4\pi r^3 \alpha_r \epsilon_{HII}}} k_b T_{HII} \quad (2)$$

where $\alpha_r \approx 4 \times 10^{-13} \text{ cm}^3 \text{ s}^{-1}$ is the recombination coefficient, and $T_{HII} \approx 10^4 \text{ K}$. Using $Q = 9 \times 10^{50} \text{ s}^{-1}$ and $r \approx 10 \text{ pc}$, we find $P_{HII} \approx 2 \times 10^{-10} \epsilon_{HII}^{-1/2} \text{ dynes cm}^{-2}$.

Second, we can use the observed X-ray flux to estimate the pressure in the hot ($T_x \sim 10^7$ K) gas. From Figure 1 in Seward et al. (1979) we estimate the radius of the diffuse X-ray emission region to be ~ 12 pc, similar to the size of the free-free emission region. Combined with the diffuse X-ray luminosity and $T_x = 6 \times 10^6$ K, this yields $n_x \approx 9 \times 10^{-2}$ and $P_x \approx 7 \times 10^{-11}$ dynes cm^{-2} , which we take to be equal to the pressure of the radio emitting gas.

The surface brightness of both the radio and X-ray emission is not uniform, indicating that the pressure is not constant inside the bubble. For example, for the two classical and smaller scale embedded H II regions Carina I and Carina II, using the fluxes and sizes from Huchtmeier & Day (1975) we find a pressure 9×10^{-10} dynes cm^{-2} . Similarly, Seward et al. (1979) estimate the density of the hot X-ray emitting gas in the prominent $r \sim 1.25$ pc diffuse patches to be $n \sim 0.4$, giving $P \approx 3 \times 10^{-10}$ dynes cm^{-2} .

Finally, we can estimate the pressure from the outflow seen to be emerging from the globule known as ‘the finger’, which has a dense ionization front and photoevaporative flow, with a terminal shock resolved close to the edge. Estimates of the ionization front density can be obtained from the S II emission line, and from the $\text{H}\alpha$ emission measure. These give electron densities of 2000-6000 cm^{-3} at various positions. The dense ionization front drives a photoevaporative flow out into the H II region until it reaches a terminal shock where the pressure is balanced with the ambient medium. To calculate P_{IF} assume the temperature is 10^4 K due to hydrogen ionization and the flow is spherical. Nathan Smith (private communication) made two estimates, one using the tip of the finger with a very small ionization front radius but a relatively high number density of 6000 cm^{-3} and a second using the main part of the fist with a larger ionization front radius and a lower density of 3300 cm^{-3} . These yield 5.4×10^{-10} dyne cm^{-2} and 7.3×10^{-10} dyne cm^{-2} , respectively.

These rather direct measurements of the pressure in several gas phases can be compared to two other pressures, the pressure exerted by the self-gravity of the surrounding molecular gas (as estimated from CO measurements) and the pressure of radiation from the stars in Tr 16 on dust grains in the interstellar medium. Yonekura et al. (2005) find a mass of molecular gas $M_g \approx 3.5 \times 10^5 M_\odot$ in a region of radius $r \approx 20$ pc, yielding a surface density $\Sigma \approx 6 \times 10^{-2}$ g cm^{-2} . Assuming this gas is in hydrostatic equilibrium (there is evidence that it is expanding outward, but we ignore this for the moment) the dynamical pressure is $P \approx \pi G \Sigma^2 \approx 8 \times 10^{-10}$ dynes cm^{-2} .

The near equality between the pressure in the X-ray gas and that of the H II gas likely reflects the fact that the sound crossing time (of the cooler gas) is similar to the dynamical time or the age of the system. Like the hot gas, the H II gas will ‘head for the exits’; pressure gradients will drive the warm gas toward any holes in the bubble shell, reducing the pressure on a (H II gas) sound crossing time.

Unlike the hot gas, the velocity of the warm gas is comparable to the velocity of the bubble wall, so a pressure driven flow will not reduce the H II pressure in the bubble by a large (factor of 10 or more) amount. Thus it appears natural that the H II gas will have a pressure similar to that estimated from the ionizing photon luminosity. Conversely, the hot gas pressure will, if it ever reaches values similar to $L_w\tau/V$, drive outflows through holes in the bubble that have velocities of order the sound speed of the hot gas, which is two orders of magnitude larger than the velocity of the bubble wall. This will lower the pressure of the hot gas until it approaches that of the H II gas, at which point the pressure gradients in the two components are similar.

Using the dynamical argument that the H II pressure and the X-ray gas pressure should be roughly equal, we can draw one more conclusion: that ϵ_{HII} is of order unity. To do so, set the right hand side of eqn. 2 equal to the (observed) pressure of the x-ray gas and solve for ϵ_{HII} , then use the known values of Q , r , and T_{HII} .

The pressure exerted by radiation is $P_{rad} = L_{bol}/(4\pi r^2 c) \approx 4 \times 10^{-10} (10 \text{ pc}/r)^2 \text{ dynes cm}^{-2}$. This near-equality, unlike that between the H II and X-ray gas pressure, is a bit of a coincidence. The radiation pressure scales as R^{-2} while the H II gas pressure scales as $R^{-3/2}$; the radiation pressure was more important in the past, while the gas pressure will become more important as the bubble expands in the future.

All of these observationally driven estimates are well below the pressure estimated by dividing the total stellar wind kinetic energy by the volume of the bubble; the latter is $P_{wind} = 3.6 \times 10^{-7} (10 \text{ pc}/r)^3 (L_w/4 \times 10^{38} \text{ erg s}^{-1}) \text{ dynes cm}^{-2}$. Either the wind has expanded over a volume larger by a factor of ~ 1000 , the wind luminosity is overestimated by a similar factor, the shocked gas loses most of its internal energy (but not by radiation in the X-ray band), or some combination of all three. We note that if the hot gas expanded at its sound speed, it would reach radii of 1 kpc, so the notion that the hot gas has expanded through holes in the ISM to occupy region with a typical size of 100 pc is not implausible.

Assuming an age of 3.6 Myrs, we find an average expansion velocity for the bubble wall of $\sim \pm 3 (R/10 \text{ pc}) \text{ km s}^{-1}$, similar to the 5 km s^{-1} splitting seen in CO (Grabelsky et al. 1988). Observations of ionized gas typically find larger velocity splittings, of order $\pm 20 \text{ km s}^{-1}$, ranging up to several hundred kilometers per second e.g. Walborn & Hesser (1975, 1982), but we regard this as a measure of the velocity of gas in the interior of the bubble, not a measurement of the velocity of the bubble wall.

To sum up, the warm and hot gas appear to be in pressure equilibrium, with a pressure $P_g \approx 2 \times 10^{-10} \text{ dynes cm}^{-2}$. This is similar to the radiation pressure, and to the pressure exerted by the surrounding, self-gravitating molecular cloud. The kinetic energy input from stellar winds greatly exceeds the integral of this pressure over the apparent size of the H II region, $R \approx 10 \text{ pc}$, suggesting that the winds have escaped to occupy a much larger volume,

or been otherwise dissipated.

3. METHODS

3.1. Chevalier and Clegg bubble

Stevens & Hartwell (2003) applied the Chevalier & Clegg (1985) steady state wind to super star clusters. The flow is assumed to pass through the sonic point at the cluster edge where the source terms become zero. The equations describing the flow are given in Appendix I.

Numerical integration of the flow (equations (A1) to (A3)) using iterative calculations of the mach number (equation (A6) or (A7)) at every step enables the flow to be accurately calculated. The X-ray luminosity from Bremsstrahlung is numerically integrated from the resulting temperature and density profiles. The actual X-ray luminosity will be somewhat larger than this estimate by about a factor of three at $T_x = 10^7$ K, see, e.g., Sutherland & Dopita (1993).

3.2. Castor bubble

In the Castor et al. theory the stars are assumed to blow a constant, spherically symmetric stellar wind that interacts with the ambient ISM and produces a bubble. For the first few hundred years the stellar wind freely expands at the wind velocity. Once the wind shocks, there is a period of adiabatic expansion for a few thousand years. The bubble then enters the “snow plough” stage when swept up mass densities reach the critical point for radiative cooling and a thin shell forms. In the Castor scenario the snow plough stage is the most readily observed phase as it is by far the longest lived. During this time the bubble has a four zone structure, (Fig. 1(i)): **a**) A hypersonic stellar wind. **b**) A hot ($T \sim 10^6$ K), almost isobaric region consisting of shocked stellar wind mixed with a small fraction of the swept-up interstellar gas. **c**) A thin, dense, cold ($T \ll 10^6$ K) shell containing most of the swept up material at R_b . **d**) Ambient interstellar gas.

One of the most important features of the snow plough structure is the cooling between zones b and c. The shell, c, is dense and cold due to efficient radiative cooling. However, zone b is hot as its density is too low to radiatively cool. Thermal conduction between b and c causes gas from the inner edge of c to evaporate into b. Although the mass loss from c is negligible compared to the accretion of mass from swept up ISM, it dominates over stellar wind as a source of matter in b. The bubble shell is pushed outward by the pressure from the confined hot gas. The equations describing the evolution are given in Appendix II.

Unlike the Chevalier & Clegg theory, the Castor theory takes into consideration the mass swept up from the surrounding nebula, requiring an ISM or GMC model. The original papers (Castor et al. 1975; Weaver et al. 1977; Chevalier & Clegg 1985) assumed a homogeneous ISM. However, in our models for Carina we sometimes employ an isothermal sphere as an approximation for the GMC surrounding the cluster. The values for the cluster gas mass and radius, and the surrounding GMC mass and radius were taken from Murray et al. (in prep) assuming a density profile in the cluster of r^{-1} and in the GMC of r^{-2} . The ‘standard’ ISM model used for our bubble models was $R_{cl} = 1$ pc, $M_{cl} = 2.6 \times 10^4 M_{\odot}$, $R_G = 24.62$ pc, and $M_G = 3.2 \times 10^5 M_{\odot}$, where M_{cl} is the mass in gas and dust remaining in the cluster after star formation assuming a star formation efficiency of $\sim 35\%$. The R_G was chosen so that the density at the boundary between the cluster and GMC was continuous.

In other cases we assume that the density falls off as $\rho(r) \sim 1/r$, or even that the density is (on average) uniform.

In the Castor models we assume that the cluster produces a point source wind from the centre of the cluster. Although this does not accurately represent the stellar wind within the cluster radius, simulations by Cantó et al. (2000) show that the approximation is valid once outside the cluster radius.

To model the Castor bubble, we used the `integrate_ode` program from Numerical Recipes (Press et al. 1996) to simultaneously integrate the momentum, radius, mass and energy evolution equations (equations (B11) to (B14)) from the initial conditions in Weaver et al. (1977) (equations (B15) to (B23)).

The X-ray luminosity was calculated taking into account the radial profile of density and temperature through the bubble (Weaver et al. 1977). When the X-ray luminosity is calculated the bubble is split into 5000 shells of equal width between R_a and R_b and the X-ray luminosity in the Einstein band from Bremsstrahlung radiation is calculated for each shell. A resolution check was conducted at many different bubble radii to ensure accuracy.

3.2.1. *Modifications to the Castor bubble model - stellar mass loss rates*

The generally accepted mass loss rate of O stars assumes a smooth (not clumpy) outflow throughout the main sequence lifetime. However, recent observations show that stellar winds are clumpy and hence the mass loss rates are likely lower than previously accepted (Fullerton et al. 2004; Bouret et al. 2005; Evans et al. 2004; Puls et al. 2006). These observations suggests that the mass loss rate is at least three times and possibly more than 30 times lower than previously expected. We introduce α to parametrize the reduction in the the mass loss rate: $\dot{M}_w = \alpha \dot{M}_{w,original}$ and $L_w = \alpha L_{w,original}$.

3.2.2. Radiation pressure

The far infrared luminosity in the direction of Carina is roughly half the total stellar luminosity. It follows that half or more of the momentum carried by light emitted by the stars is deposited into the gas near the stars. Thus, the radiation pressure contributes to the outward force on the bubble shell (where the UV optical depth is large)

$$F_{rad} = \eta \frac{L_{bol}}{c}, \quad (3)$$

where η is of order 1/2, c is the speed of light and L_{bol} is the total bolometric luminosity from the cluster.

Using a multi-wavelength analysis of the Carina Nebula Smith & Brooks (2007a) estimate dust temperatures and calculate the total mass in dust. Smith & Brooks (2007a) calculate the masses using the models of Gilman (1974). We employed more recent dust models (Laor & Draine 1993); the mass in dust can be calculated using the mass per grain, $4\pi a^3 \rho / 3$ and luminosity per grain = $Q_e \sigma T_d^4 4\pi a^2$

$$M_d = \frac{a\rho}{3\sigma Q_e T_d^4} L_d, \quad (4)$$

where a = effective grain radius, σ is the Stefan-Boltzmann constant, Q_e = mean thermal emissivity, T_d = dust temperature, and L_d = the dust luminosity. No silicate features are seen so we can assume the grains are carbon. We also assume that grains are small ($a < 0.2\mu\text{m}$). The Q_e values for each temperature can be read from the graph in Laor & Draine (1993). In particular, $Q_e \approx 3 \times 10^{-3}$ for $T_d = 35$ K. This is factor of 9 larger than the value employed by Smith & Brooks (2007a); consequently, we find a total dust mass $M_d \approx 1000(\rho/3 \text{ g cm}^{-3})M_\odot$, Table 2, a factor 9 smaller than Smith & Brooks (2007a).

Assuming a dust to gas ratio of 1:100 the total mass for the surrounding nebula is $\sim 10^5 M_\odot$, corresponding to an $A_V \approx 1 (20 \text{ pc}/R_b)^2$. In contrast, Smith & Brooks (2007a) find $9.6 \times 10^5 M_\odot$, corresponding to an $A_V \approx 10 (20 \text{ pc}/R_b)^2$.

Smith & Brooks (2007a) find $T_D \approx 35$ K, which we argue supports the lower mass estimate, as follows. Using the expression for dust temperature

$$T_d = 49 f^{-1/(4+\beta)} \left(\frac{2 \times 10^{17} \text{ cm}}{r} \right)^{2/(4+\beta)} \left(\frac{L_{bol}}{10^5 L_\odot} \right)^{1/(4+\beta)} \quad (5)$$

from Scoville & Kwan (1976) with $f = Q_{abs}(\lambda = 50\mu) \approx 0.01$ we find that the typical distance between a dust grain and Tr 16 is ~ 24 pc (taking $\beta = 1$). We note that this is similar to the estimated bubble size. Since the bulk of the stellar radiation is initially emitted in the UV, it will be absorbed at $A_v \lesssim 1$, consistent with the lower mass estimate given above.

3.2.3. Self-Gravity

As the shell sweeps up a substantial amount of mass, the self-gravity of the shell and gravity between the shell and the stars and interior gas should be considered in the momentum equation.

$$F_{grav} = -\frac{GM_c^2}{2R_b^2} - \frac{GM_c(M_b + M_{stars})}{R_b^2}. \quad (6)$$

3.2.4. Leakage of hot gas

The Castor theory assumes expansion through an homogeneous ISM. However, as noted in the introduction, turbulence is expected to produce density fluctuations in the ISM, while observations show that the column density is log-normally distributed. Thus, sections of the bubble shell with low column will expand faster and high column sections will expand more slowly. This uneven expansion will result in gaps in the shell, allowing the hot gas to escape from the bubble.

We investigated the effects of holes in the expanding shell using a toy model. Our model consisted of a Castor-style bubble with a shell cover fraction C_f : when $C_f = 1$ the shell has no holes and when $C_f = 0$ the shell is covered with holes, i.e. no shell exists. These holes allow the interior gas to escape at the speed of sound, $c_s = (5k_bT/(3m_p))^{1/2}$, with a mass flux and energy flux given by

$$\dot{M}_b = -(1 - C_f)4\pi R_b^2 \rho_b c_s, \quad (7)$$

$$\dot{E}_b = -(1 - C_f)4\pi R_b^2 \frac{5}{2} \rho_b c_s^3, \quad (8)$$

where R_b is the radius of the bubble interior, ρ_b is the density inside the shell, which is assumed to be homogeneous and $\gamma = 5/3$ through this paper.

We are not concerned with the bubble evolution within the cluster radius (of order 3 pc for Tr 16). Thus, we neglect gravity and radiation pressure for $r < R_{cl}$; once the bubble expands, under the influence of the other forces, beyond this radius, we smoothly turn on gravity and radiation pressure.

With hot gas from the interior able to leak away, it is important to consider the location of the stellar wind shock, R_a (see Fig. 1): if R_a approaches the shell radius at any time our model breaks down. We use the assumed ambient ISM density profile for the regions where the shell is still intact and negligible density where there are holes. Although this is not an accurate description of a clumpy ISM, it does allow the shell to leak while still gaining mass as it expands through a variable density ISM. The gas and radiation pressure only acts on the remaining shell (i.e. area = $C_f 4\pi R_b^2$).

Without leaking the radiative losses in region b were negligible. However, with leaking this may not always be the case. To ensure these losses are taken into account when significant we calculate the radiative luminosity of region b, L_b , and include it in the energy equation.

The sizes of the holes in the shell may vary as the bubble expands, so that $C_f = C_f(t)$ or $C_f(r)$. To investigate the effects of different hole expansion models, we conducted runs with many different power law relationships with time (including $C_f(t) = \text{const.}$), which we discuss below.

3.2.5. Final bubble model

Considering radiation pressure, gas pressure, stellar winds, gravity and leaking the evolution equations for momentum, radius, mass and energy become

$$\frac{d\mathcal{P}_c}{dt} = 4\pi R_b^2 P_b + \frac{L_{bol}}{c} - \frac{GM_c^2}{2R_b^2} - \frac{GM_c(M_b + M_*)}{R_b^2}, \quad (9)$$

$$\frac{dR_b}{dt} = \frac{\mathcal{P}_c}{M_c}, \quad (10)$$

$$\frac{dM_b}{dt} = C_1 T_b^{5/2} R_b^2 (R_b - R_a)^{-1} - 10^{-5} \frac{\mu}{k_b} L_b - (1 - C_f) 4\pi R_b^2 \rho_b c_s, \quad (11)$$

$$\frac{dE_b}{dt} = L_w - 4\pi R_b^2 P_b \frac{dR_b}{dt} - L_b - \frac{5}{2} (1 - C_f) 4\pi R_b^2 \rho_b c_s^3. \quad (12)$$

respectively, see Fig. 1(ii).

\mathcal{P}_c is the momentum of the shell, t is time, R_b is the radius of the bubble, P_b is the gas pressure in the bubble interior, L_{bol} is the total bolometric luminosity of the stars, c is the speed of light, G is the gravitational constant, M_c is the mass of gas in the bubble shell, M_b is the mass of gas in the bubble interior, $M_* = 10^4 M_{sun}$ is the mass of stars in the cluster, C_1 is a combination of constants associated with conduction, T_b is the temperature of the gas in the bubble interior, R_a is the radius of the stellar wind shock, k_b is the Boltzmann constant, L_b is the luminosity emitted from the bubble interior, C_f is the covering fraction of the shell, ρ_b is the mass density of the bubble interior, c_s is the speed of sound of the bubble interior, E_b is the energy in the gas in the bubble interior, L_w is the stellar wind luminosity.

The terms on the right hand side of the momentum equation (9) represent, in order, the outward force from the gas pressure, the outward force from radiation, the inward force from the self gravity of the bubble shell, and the inward force from gravity between the star cluster (with a minor contribution from the gas in the bubble interior) and the bubble shell. The terms on the right hand side of the mass equation (11) are the mass input associated with

conduction evaporating the bubble wall, a (downward) correction in the conductive mass loss rate associated with radiative cooling, and mass loss from hot gas escaping the bubble. The terms on the right hand side of the energy equation (12) are stellar wind luminosity, adiabatic expansion, radiative cooling, and energy advection associated with the loss of hot gas through the bubble wall.

4. RESULTS

4.1. Original stellar wind models

The Chevalier & Clegg model predicts a free-free X-ray luminosity in the Einstein band (0.5 – 3 keV) of $L_x = 3.75 \times 10^{33} \text{ erg s}^{-1}$ for Carina. The Castor model predicts an X-ray luminosity of $L_x = 5.4 \times 10^{36} \text{ erg s}^{-1}$ for $R_b = 13 \text{ pc}$ and $L_x = 3.8 \times 10^{36} \text{ erg s}^{-1}$ for $R_b = 20 \text{ pc}$. Plots of the models can be seen in Fig. 2 and Fig. 3. Both of these models considered X-ray emission from $r > R_{cl}$ to match the observations, in which the cluster region is ignored due to contaminating stellar and wind-wind collisional X-ray emission.

In the Chevalier & Clegg model the inner region of the wind dominates the X-ray luminosity so a strong radial gradient in the X-ray surface brightness is predicted; beyond a few parsecs the X-ray luminosity is negligible. In contrast, in the Castor et al. model the density is almost homogeneous within the bubble, so very little radial surface brightness gradient is expected, aside from a sharp edge at R_b .

Observations of diffuse X-ray emission in Carina give $L_x = 6.1 \times 10^{34} \text{ erg s}^{-1}$ (Seward et al. 1979); those authors assumed the distance to the cluster was 2.6 kpc. If we assume the distance is 2.3 kpc, the luminosity becomes $4.8 \times 10^{34} \text{ erg s}^{-1}$. The observed X-ray emission is ten times higher than predicted by Chevalier & Clegg model but one hundred times lower than predicted by the Castor model, Fig. 4. The observed pressure, as estimated by ‘the finger’ and radio emission, is closer to the calculated Castor pressure when the bubble has the currently observed radius $R_b \approx 20 \text{ pc}$.

As noted elsewhere, the Chevalier & Clegg model predicts a pressure that has a strong radial gradient, so the pressure is dependent upon the location within the bubble rather than the bubble size. However, the Chevalier & Clegg pressure is far below the observed pressure at most points in the bubble.

It is unclear how long it takes the bubble to reach the cluster radius, as the expansion time will depend upon the rather complicated wind-wind interactions within the cluster. To properly understand the early evolution of bubbles, full hydrodynamical models are needed. However, for now we will assume it is much less than a million years, as material will be displaced during star formation due to pre-main sequence jets and outflows. We assume

that the majority of the time taken to expand to the observed size is accumulated when $R_{cl} < r < R_{obs}$. Using this assumption we found that to expand to 20 parsecs the Castor model took only 0.90 million years, far shorter than the estimated age of Carina (around 3.6 Myrs).

It follows that the situation for the Castor et al. model is actually worse than the impression conveyed by the Figure, for the following reason. The actual age of the bubble is a factor of four higher than in the model, so the energy content of the bubble is underestimated in the model by the same factor, as is the pressure. Given the weak dependence of the temperature on time, the X-ray luminosity scales as the square of the pressure; if the radius, wind luminosity, and age of the bubble are set by observations, then the X-ray luminosity would be a factor of 16 larger than in the model.

4.2. Modified Castor et al. model; leakage

Taken together, the overestimate of the pressure and X-ray flux, and the underestimate of the bubble age (or overestimate of the bubble size at a fixed age) suggest that the outward force in the Castor et al. model is overestimated.

The inclusion of radiation pressure and gravity for the Tr 16 model makes only a small difference to the evolution of the bubble. For Tr 16 $|F_{HII}| \approx |F_{RP}| \approx |F_{grav}|$; in the model, unlike the case in Carina, all are much smaller than the gas-pressure force exerted by the shocked stellar wind, assuming no leakage and a standard O star mass-loss rate.

In an attempt to produce models in closer agreement with observations, it is clear that the internal pressure of the bubble must be reduced. One way to do this is to allow hot gas to leak out of the bubble ($C_f < 1$), or equivalently to allow energy to leak out of the hot gas, via radiation or conduction; another is to reduce the mass loss rate and hence the kinetic luminosity of the stellar winds ($\alpha < 1$).

Observation of massive clusters support the possibility of leaking. Firstly, for Carina and many other clusters you can see the stars, showing that there must be a gap in the shell along our line of sight (Smith & Brooks 2007b). Secondly, recent observations of M17 and RCW49 by Povich et al. (2008) show stellar wind bow shocks around O stars at the edge and outside of the bubbles suggestive of large scale gas outflow from the H II region (see their Figure 2, especially RCW49-S1).

Our initial simulations of a leaking bubble looked at three examples in detail: $C_f = 1.0$, $C_f = 0.65$, and $C_f = 0.3$. The results are given in Fig. 5. Not surprisingly, these simulations reveal that as C_f decreases the shell expands more slowly, the bubble interior pressure is lower, as is the predicted X-ray luminosity.

The effects of varying C_f with time were then investigated. These simulations started with $C_f = 0.6$ at $t = 10^3$ years and evolved $C_f(t)$ with different power laws until $t = 3\text{Myrs}$, when $C_f = 0.2$. The simulations show that expansion rate, pressure, temperature and density differ very little with different power-law exponents; however, the X-ray luminosity does depend on the exponent. The difference in X-ray luminosity is due to the combination of the small changes in the parameters giving larger X-ray luminosities for larger exponents; larger exponents imply C_f being large for longer times. Thus, less material escapes over the lifetime of the bubble: $\dot{M}_{escape} \propto (1 - C_f)$ and the X-ray luminosity is higher during the expansion when the power-law exponent is larger.

To see the way C_f and the run of density in the ISM affected the evolution of the bubble we ran four different models. We considered $C_f = 1.0$ or 0.5 and either isothermal or constant density models (with the same total mass), Fig. 6. From this study we find that a homogeneous medium leads to a faster expansion; the mass swept up in the bubble shell is less at a given radius in the constant density model. However, the isothermal sphere model does approach the homogeneous model near the end of the simulations when both reach R_G and hence the same shell mass. The models with $C_f = 0.5$ expanded more slowly and had significantly lower X-ray luminosities than models with $C_f = 1.0$, as expected.

We conducted a parameter study in α and C_f to see if any combination would result in acceptable fits to the observed bubble in Carina. Models were calculated for $0.15 \leq C_f \leq 0.99$ and $0.01 \leq \alpha \leq 1.00$, stepping both parameters at intervals of 0.01. The results are shown in Fig. 7; contours are only plotted for $R_b < 50$ pc at a bubble age of 3 Myrs. This parameter space study was run for four different ISM models. Runs shown in part (a) of the Figure are for an isothermal sphere model with $R_G = 24$ pc; run (b) shows an constant density model with $R_G = 24$ pc; run (c) is for an isothermal sphere model with $R_G = 60$ pc; and run (d) is for a constant density model with $R_G = 60$ pc.

The results show that isothermal sphere models gives smaller radii and slightly higher X-ray luminosity for any given (α, C_f) pair. The final radius at 3 million years increases with increasing α and with increasing C_f , as expected. For the isothermal ISM model the shell actually collapses inwards for low values of α and low values of C_f , a result of the self gravity of the shell exerting an inward force larger than the sum of the gas pressure force and radiation pressure force on the shell.

The X-ray luminosity increases with increasing α and increasing C_f , again as expected. The region of parameter space that best fits the observations is for an isothermal sphere model with $R_G = 60$ pc. For this class of model there is a large parameter space with R_b between 10 and 20 parsecs and X-ray luminosities less than 4.8×10^{34} erg s $^{-1}$. For example, for $\alpha = 0.2$ and $C_f = 0.5$, $R_b = 16.5$ pc, $L_x = 1.2 \times 10^{34}$ erg s $^{-1}$, and $P_b = 1.1 \times 10^{-10}$ dynes cm $^{-2}$.

5. X-RAY SURFACE BRIGHTNESS PROFILES

The morphology of the X-ray emission provides a diagnostic to test our models. Matching up the X-ray emission (Hamaguchi et al. 2007a) and the visual images of the Carina nebula (Smith & Brooks 2007b), Fig. 8, it can be seen that the X-ray surface brightness increases near the edge of the bubble, the latter seen as a silhouette in the visible image. This strongly suggests that a significant fraction of the diffuse X-ray emission seen by Seward et al. (1979) was produced by gas evaporating from the bubble wall.

This surface brightness profile is not predicted by either the Chevalier & Clegg (1985) or Castor et al. (1975) models; the former predicts that surface brightness falls monotonically with increasing r , while the latter predicts a nearly flat surface brightness profile out to $r = R_b$. For an example of the latter, consider one run with $\alpha = 1/3$, $C_f = 0.5$, an isothermal sphere ISM with $R_G = 60$ pc, and stellar wind, radiation pressure, and gravity all included. At an age of 3 Myrs we find a bubble radius of 34 pc and a total X-ray luminosity of 1.3×10^{34} erg s⁻¹, roughly consistent with the observed bubble. The cumulative X-ray emission as a function of the 3D (not projected) radius is shown in Fig. 9(a); the X-ray profile with 2D (projected) radius is shown in Fig. 9(b). The calculated profiles show an almost flat X-ray profile with a sharp edge at the bubble boundary. This contrasts with the Seward et al. (1979) and more recent XMM images (Hamaguchi et al. 2007a), which are much more complex, with an elevated surface brightness near the bubble walls as noted above.

5.1. Globule evaporation

To estimate the emission from the interface between the hot stellar wind material and the molecular gas around the bubble, we first look at a simplified case of a spherical globule of cold gas embedded within the hot gas of the bubble interior, the latter having temperature T_f and number density n_f at large distances from the cold globule. The cold gas will be heated by conduction and evaporate, as discussed in, e.g., Cowie & McKee (1977). The theory makes three assumptions; firstly the globule is large enough to give a roughly time-independent solution for the mass loss rate, secondly that the thermal conduction is unsaturated, and thirdly that the flow has a moderate Mach number ($\mathcal{M}^2 \ll 5$). The conduction is unsaturated if the thermal mean free path for electrons is much shorter than the temperature scale height. For the Carina nebula, with $n_x \approx 0.1$ cm⁻³ and $T_x = 6 \times 10^6$ K, the conductivity is approaching the saturated limit for globule radius $R_1 \approx 1$ pc. Assuming we are in the unsaturated case, the mass loss rate is given by the classical equation (same

as equation 2)

$$\dot{m} = \frac{16\pi\mu K(T)R_1}{25k_b} \quad (13)$$

where μ is the mean mass per particle, $K(T)$ is the conductivity at T_f , and R_1 is the radius of the globule. The dimensionless form of the equation of motion is

$$(1 - \mathcal{M}^2) \frac{d \ln \mathcal{M}^2}{dy} = \frac{2(6 - 5y) + \mathcal{M}^2 - 1}{2.5y(y - 1)}, \quad (14)$$

where \mathcal{M} is the mach number of the flow and $y = r/R_1$. We assume that the flow will shock somewhere close to the sonic point and thus still satisfy $\mathcal{M}^2 \ll 5$ at all radii.

The solution of the energy equation gives the temperature profile

$$T(y) = T_f (1 - y^{-1})^{2/5}, \quad (15)$$

assuming the globule temperature $T \ll T_f$. The local sound speed can be calculated from the temperature profile and thus the velocity deduced from the local Mach number. The local density is then

$$n(y) = \frac{\dot{m}}{4\pi y^2 R_1^2 c_s \mathcal{M}}. \quad (16)$$

The run of temperature and density can be combined with the expression for Bremsstrahlung X-ray emission to give the expected X-ray luminosity and surface brightness for an evaporating globule. The intensity along a line of sight with an impact parameter b to a globule is proportional to

$$\int dz n^2(z) T^{1/2}(z) e^{-kT/h\nu} \approx \int dz \frac{T^{1/2}(r(z))}{(b^2 + z^2)^2} e^{-kT/h\nu} \sim \left(\frac{R_1}{b}\right)^3 \quad (17)$$

where z is measured along the line of sight, $z = 0$ in the plane of the sky at the location of the globule, and $r = \sqrt{b^2 + z^2}$. Once $T(r)$ approaches $h\nu/k$, the surface brightness depends primarily on b , falling rapidly with increasing b as long as $R_1 < b$. Doing the integral numerically, setting $T_f = 6 \times 10^6$ and $R_1 = 1$ pc we get $\dot{m} = 6 \times 10^{21}$ g s⁻¹ and the X-ray emission profile shown in Fig. 10; the dotted line shows the b^{-3} scaling. In words, a spherical globule should be surrounded by a fairly sharply defined X-ray halo.

As a check, the dependence of the total X-ray luminosity and mass loss rate on T_f and R_1 were investigated. We varied the external temperature for a globule of $R_1 = 1$ pc; in a separate set of integrations at fixed $T_f = 10^6$ K we varied the radius of the globule R_1 . These simulations show that $\dot{M} \propto T^{2.5}$, $L_x \propto T$, and $\dot{M} \propto T$ as expected analytically for an unsaturated conductivity.

A very crude calculation of the X-ray emission produced by the conductive evaporation of a collection of globules forming the bubble wall suggests that most or all of the X-ray emission could arise in this manner:

$$L_x = \int 4\pi r^2 \Lambda_x n^2(r) dr. \quad (18)$$

Using eqn. (16),

$$L_x \approx 4\pi \Lambda_x \left(\frac{\dot{m}}{4\pi c_s m_p} \right)^2 \frac{1}{R_1} \approx 2.6 \times 10^{33} \left(\frac{R_1}{1 \text{ pc}} \right) \left(\frac{\Lambda_x}{3 \times 10^{-23} \text{ erg s}^{-1} \text{ cm}^3} \right) \text{ erg s}^{-1}. \quad (19)$$

If the bubble wall (or about half of it) were tiled with $R_1 \sim 3 \text{ pc}$ globules, evaporation from the wall could explain the observed X-ray emission.

In Carina the situation is much more complicated than this toy model. The density of the hot gas is manifestly not uniform, and in addition we have seen that hot gas apparently escapes rapidly from the bubble interior. We are assuming that this implies that the gas density decreases rapidly away from the bubble wall, on a scale comparable to the size of the wall fragments, which are typically much smaller than the radius of the bubble. Further work along these lines is clearly needed.

We have extracted surface brightness profiles along rays emanating from η Carina using the XMM observations of (Hamaguchi et al. 2007a). The southern part of the XMM image is shown in Fig. 11, which also shows the three rays along which the surface brightness was calculated for Fig. 12. These profiles were produced by interpolating through the pixels using IDL and then smoothing. All three lines were interpolated through 2554 points and then smoothed by a box car average with a width of 60 points.

Emission was converted from counts to flux using the PIMMS package. We assumed a spectrum of two black bodies as found by Hamaguchi et al. (2007a).

The 700-1300eV band shows the greatest contrast, from little emission in the bubble interior (but away from η Carina) to substantial emission near the optically dark lanes. The 400-700eV band also shows some edge effects, especially along lines Two and Three. The high energy band, 2000 – 7000 eV, shows essentially no enhanced emission near the bubble walls.

In the 700-1300eV band line One shows a decrease in surface brightness from η Carina out to 200 arcsec, a fairly flat profile between 200 and 650 arcsec, followed by a decrease out to the edge of the image. Line Two shows a similar flat profile between 150 and 400 arcsec, decreases to a minimum surface brightness at 500 arcsec, then increases to a peak at about 900 arcsec. The profile along line Three is similar to line two but with a less pronounced minimum, and a peak closer to η Carina (at 750 arcsec). The peak along ray Three is wider

than that along ray Two as it makes a larger angle with the bubble edge normal. These profiles quantify the visual impression that the bulk of the bubble interior has a fairly flat X-ray surface brightness but that there is strong emission from the edges. The edge profiles are of significantly different shape to that expected from a Castor bubble, Fig. 9(a) and are more curved than would be expected from globule evaporation, Fig. 10.

6. DISCUSSION

We have noted three discrepancies between the Castor et al. scenario and observed bubbles: the predicted bubble radii are too large at a given cluster or stellar age, the predicted X-ray luminosities are too high by a factor of 100 or more, and concomitantly, the predicted pressure of the hot gas is too large by a factor of 10 or more. Finally, we have noted that the radio free-free emission is consistent with a filling factor of H II gas that is of order unity, suggesting that the pressure in the bubbles is controlled by the H II gas rather than that of the shocked stellar wind gas.

A number of authors have noted the small observed R_b , roughly by a factor of 5, compared to predictions (Dorland, Montmerle, & Doom 1986; Dorland & Montmerle 1987; Oey 1996; Rauw et al. 2002; Dunne et al. 2003; Smith, Struck, & Nowak 2005). These authors have also noted the deficit of X-ray luminosity or hot gas pressure compared to predictions. Suggested resolutions involve one or more of the following: lower stellar wind luminosities, mass loss from the bubble, or energy loss from the bubble, e.g., from super-Spitzer effective conductivities, or highly efficient mass loading so that the shocked stellar wind cools by conduction below X-ray temperatures.

Castor et al. (1975) and Weaver et al. (1977) make three assumptions; first, that the energy deposited by the stellar winds (or 5/11 of it) is stored in the hot gas inside the bubble, second, that the hot gas mass is controlled by conduction (at the Spitzer rate), and third, that the surrounding ISM is uniform (represented by their constant density n_0). Applying the model requires knowledge of L_w , n_0 , and the age of the system. The predicted bubble radii depend only weakly on L_w and n_0 , while the ages of star clusters are reasonably well constrained (to within a factor of 2–4). Since the bubble radii are universally overestimated, at least one assumption must be incorrect.

We can acknowledge the fact that the dynamics of the model are wrong, but still test the first assumption, that the energy deposited by the stellar winds is stored inside the bubble. We will also assume that conduction drives gas from the bubble wall into the interior until $T_b \sim 10^6 - 10^7$ K; this assumption is bolstered by the observed gas temperatures, which cluster around 6×10^6 K.

The argument is that the time integrated wind luminosity deposits an energy $E = (5/11)L_w\tau$ in the bubble interior, and that the corresponding pressure is $2E/3V$, where the volume is assumed to be a sphere with the observed bubble radius. Together with the assumption that the temperature is $T \approx 5 \times 10^6$ K, we can calculate the mean density and hence the X-ray luminosity.

Both X-ray and other observations give estimates of the bubble radius. Star counts (to a given limiting magnitude) and radio observations give estimates of L , the bolometric stellar luminosity, or Q . The stellar wind luminosity can then be estimated from either L or Q , with the caveats mentioned above. Finally, from the presence of Wolf-Rayet stars and/or SN remnants, we have estimates of the cluster age. In terms of these quantities, the X-ray luminosity is

$$L_x \approx 3 \times 10^{38} \xi \left(\frac{L_w}{4 \times 10^{38} \text{ erg s}^{-1} \text{ s}^{-1}} \right)^2 \left(\frac{20 \text{ pc}}{r} \right)^3 \left(\frac{6 \times 10^6 \text{ K}}{T} \right)^2 \left(\frac{3.6 \times 10^6 \text{ yr}}{\tau} \right)^2, \quad (20)$$

where we have assumed an X-ray cooling rate $\Lambda_x \approx 3 \times 10^{-23} \xi \text{ erg s}^{-1} \text{ cm}^3$, e.g., Chu et al. (1995), ξ is the metallicity relative to solar, and τ is the age of the cluster. We have scaled to values appropriate to Carina. As previously noted, this is 10,000 times too high.

In addition to Carina, we have calculated this predicted X-ray luminosity for the LMC H II regions detected in X-rays by the *Einstein* satellite, and discussed in Chu & Mac Low (1990). We estimate the bolometric luminosity of the H II regions in two ways. First, we use the star counts from Lucke & Hodge (1970); these authors report star counts for stars with $m_V < 14.7$, about $M_V = -3.85$ at the distance of the LMC. Second, we use the observed radio free-free flux from McGee, Brooks, & Batchelor (1972) to estimate Q and thence L ; the results from the two methods are consistent, within a factor of 3 or so. As in the case of Milky Way bubbles, this indicates that the filling factor of the H II gas is of order unity, and hence that the pressure in these bubbles is not set by the X-ray emitting gas. From the bolometric luminosity we then estimate L_w . Using these values, eqn. (20) over-predicts the X-ray luminosity, by factors ranging from a few to five hundred.

Thus the picture for the LMC is consistent with our finding for Carina. Confusingly, other authors have found an *excess* of observed X-ray emission compared to predictions of the Castor et al. model (Chu & Mac Low 1990; Chu et al. 1995; Wang & Helfand 1991). Why should this be?

Chu & Mac Low (1990); Chu et al. (1995) and Wang & Helfand (1991) all use the scaling laws of Castor et al. to predict the X-ray luminosity of bubbles in the LMC. The latter two give expression for L_x that appear to contain only directly observed quantities, such as the bubble radius and the bubble expansion velocity. However, the coefficient relating L_x to the observed quantities depends on the theoretical estimate for the bubble radius and central

bubble density. This dependence results in an estimate for the stellar wind luminosity that is more than a factor of 10 smaller than the wind luminosity as estimated from either simple star counts, or from the free-free radio emission.

In the case of Chu & Mac Low (1990), this can be seen explicitly in their discussion of N51D, where they infer $L_w = 1.08 \times 10^{37} \text{ erg s}^{-1}$ in their appendix B section IV. From the star counts of Lucke & Hodge (1970) we estimate $L_w = 2 \times 10^{38} \text{ erg s}^{-1}$; from the radio flux from McGee, Brooks, & Batchelor (1972) we find $L_w = 6 \times 10^{37} \text{ erg s}^{-1}$. Using the lower value, and the observed $R_b = 48 \text{ pc}$ eqn. (20) yields $L_x = 1.6 \times 10^{36} \text{ erg s}^{-1}$, about a factor 5 larger than the observed $L_x = 3.3 \times 10^{35} \text{ erg s}^{-1}$.

Since their estimates of L_x are smaller than the observed X-ray luminosities, Chu & Mac Low (1990) suggest that the X-ray emission of the LMC objects is provided by supernovae that have gone off near the bubble wall. We argue that, using the estimate given here, recourse to supernovae is unnecessary. In addition, the morphology of the X-ray emission in Carina does not support this picture, nor does that of the objects studied by Chu & Mac Low (1990) in the LMC. In Carina, as stated above, the emission is slightly enhanced near the bubble walls, but not at a particular point, as would be expected following a supernova.

Similarly, the X-ray images presented by Townsley et al. (2006) of N 157 (30 Doradus), especially their Figures 14 and 15, generally show rather diffuse emission in the cavities surrounded by cold dusty gas, reminiscent of what is seen in Carina. However, as Townsley et al. (2006) also remark, in some cases the emission comes from the interior of the cavity, while in others it comes from edge brightened regions with distinct central voids, similar to Carina. Two exceptions may be the regions referred to as numbers 5 and 9, which Townsley et al. (2006) suggest may be the result of supernovae interacting with the bubble wall, a la Chu & Mac Low (1990).

6.1. Dynamics Controlled by H II Gas

As we noted in section §2, the H II gas pressure in Carina, as estimated from the radio free-free emission, is similar to the pressure in the X-ray emitting gas; both are similar to the pressure where the outflows from photo-dissociation regions shock. This was pointed out earlier by Dorland & Montmerle (1987). Since the sound speed of the cooler gas is comparable to the bubble expansion velocities observed, this is not surprising.

What is more surprising is that the free-free luminosity is consistent with a filling factor for the H II gas that is of order unity (see eqn. 2) a fact apparently not noted before. This implies that the gas pressure is set by the H II gas rather than the hot gas. It suggests that the shocked stellar winds escape from the partially confining bubble at the sound speed of

the hot gas, as long as the pressure in the hot gas exceeds the H II gas pressure in the region. When enough hot gas has escaped that $P_x \approx P_{HII}$, the escape will slow, as the hot gas is impeded by the cooler gas. This sets up a rough pressure balance between the hot and H II gas.

Dorland, Montmerle, & Doom (1986) and Dorland & Montmerle (1987) consider the loss of wind energy (by an enhanced conduction by a non-Maxwellian tail of high energy electrons, according to the latter). Dorland & Montmerle (1987) note that the thermal energy in hot gas in the Rosette as well as the Carina nebula cavities is well below that input by stellar winds over the age of the respective star clusters. These authors suggest that the excess energy is conducted away from the hot gas to surrounding cold gas, rather than by simply flowing out through holes in the bubble wall as suggested here and elsewhere. This would alleviate the dynamical problem (the predicted bubble radius would be smaller than in the Castor et al. theory) and the X-ray luminosity problem.

In a similar vein, McKee, Van Buren, & Lazareff (1984) consider the evolution of wind blown bubbles in conjunction with H II regions. Like us, they conclude that the pressure and hence the dynamics of the bubble are controlled not by the 10^7 K gas, but by the H II gas. They suggest that the energy density of the shocked wind is dissipated in situ, rather than leaving the bubble. In the case of a high wind luminosity (as in Carina), they suggest that the hot gas will engulf a large number of globules, producing a large mass loading and resultant catastrophic radiative cooling.

Examination of the Hubble Carina mosaic (Smith & Brooks 2007b), which has a spatial resolution of $\sim 10^{-3}$ pc, does not reveal a large population of evaporating globules in the interior of the bubble. If the bubble wall consists of a large number of sub-resolution globules it might be possible to dissipate the wind luminosity; the bulk of the wind luminosity would be radiated near or just beyond the Lyman edge, or possibly as optical light. Radiation beyond the Lyman edge would be hard to detect due to absorption along the line of sight to Earth, while optical emission would be hard to distinguish from emission associated with ionizing radiation from the star clusters. However, preliminary calculations of the emission region associated with an evaporating globule suggest that a few percent of the luminosity would emerge in the X-ray band; only if the globules are ~ 100 AU in radius is the fraction of emission emerging in the X-ray band small enough to escape detection. The conduction around such globules is highly saturated; in fact, the mean free path for electrons to thermalize is $\lambda \sim 0.1$ pc. Hence, the globules would have to be separated by many times their own radii to avoid an X-ray emission fraction larger than observed. These small globules are surrounded by a saturated conduction region roughly ten times their own radius; if these saturated conduction regions overlap they will radiate X-rays like a single, much larger globule. We defer further discussion of this possibility to a later publication.

Neither Dorland, Montmerle, & Doom (1986) nor McKee, Van Buren, & Lazareff (1984) explain why $P_{HII} \approx \sqrt{3Q/4\pi R_b^2 \alpha_r}$ (where the latter assumes a filling factor near unity). It is not clear why the energy-loss rate of the hot gas would tune itself so that the filling factor of both warm and hot gas is near unity. A large cooling luminosity would lead to an essentially complete absence of hot gas, while a low cooling luminosity would result in too high a hot gas pressure. Unlike a simple mass loss scenario, an energy loss scenario requires some fine tuning to match the observations.

Finally, we note that our leaky bubble models, which predict smaller bubble radii and gas pressures, have implications for the prediction of spectral energy distributions of starburst galaxies. As pointed out by Dopita et al. (2005), using a standard Castor et al. bubble model results in ionization parameters too small (by a factor of 10 or more) than that inferred from spectral energy distributions of such galaxies. Both the smaller radii and the lower gas pressure (hence gas density) will increase the ionization parameter associated with bubbles surrounding massive star clusters.

6.2. Ballistic Bubbles

In the Castor et al. scenario, if the shocked stellar wind gas from a star or star cluster was confined to a bubble of volume V , the pressure of the hot gas would be

$$P_x = \frac{2}{3} \frac{5}{11} \frac{L_w \tau}{V}, \quad (21)$$

where the energy in the bubble $E_b = (5/11)L_w \tau$ and τ is the age of the star cluster. As already mentioned, this pressure is orders of magnitude larger than the observed pressure in Carina, so the hot gas is not currently exerting the predicted pressure on the surrounding dense gas.

However, it is possible that in the past the hot gas was confined. The force exerted by the gas on the bubble would have been much larger than that exerted by the H II gas or by radiation, resulting in a nearly impulsive expansion of the bubble. After this early impulsive phase, the hot gas could then leak out of the bubble, leaving the bubble to expand in a nearly ballistic manner. This could happen, for example, if the density of the trapped hot gas grew large enough that the radiative cooling time scale became shorter than the expansion time scale (Shull 1980). We argue that this is not the case.

First, high resolution radio images of ultracompact H II (UCHII) regions ($R \sim 0.1$ pc) by De Pree et al. (2005) show that most are either shell-like (see Fig. 13) or cometary (a significant fraction are bipolar). The former two would allow hot gas to leak out of the UCHII region. Observations show that the expansion velocities are typically ~ 10 km s⁻¹,

e.g., (Chakraborty & Anandarao 1997, 1999). The expanding shell will sweep up mass; if the motion is ballistic the velocity will decrease and the bubble will never reach sizes of order 10pc.

Second, there are UCHII regions that emit diffuse X-rays, e.g., in the Welch ring of W49 (Tsujiimoto et al. 2006) and in the Hourglass region of the Lagoon nebula, M8 (Rauw et al. 2002). In both cases the X-ray luminosity is well below that expected under the assumption that the shocked wind gas is confined in a bubble; it is also well below L_w . We discuss each source in turn.

The W49 ultracompact ($r \sim 0.15$ pc, $D = 11.4$ kpc) source G_X has $L_x \approx 3 \times 10^{33}$ erg s^{-1} and $T \approx 7$ keV (Tsujiimoto et al. 2006), much hotter than the plasma in Carina. The high temperature of the X-ray gas is difficult to reconcile with the Castor et al. model; such hot gas is more likely to occur in a wind-wind collision. If this is the case, then the luminosity of any truly diffuse, shocked, partially confined gas is even smaller than the value given here. The column toward the source is $\Sigma \approx 0.8$ g cm^{-2} , suggesting a dynamical pressure $P = \pi G \Sigma^2 \approx 10^{-7}$ dynes cm^{-2} , and a mean cold gas density $\rho \approx 2 \times 10^{-18}$ g cm^{-3} . This is consistent with their estimated hot gas pressure based on the emission measure ($n_x \approx 10$ cm^{-3} , $P_x \approx 10^{-7}$ dynes cm^{-2}). They suggest the driving source is one or two O5 or O6 stars, with a luminosity in the range $2 - 6 \times 10^5 L_\odot$, consistent with the ionizing photon luminosity $Q \approx 10^{49}$ s^{-1} for each of the five G sources listed by De Pree et al. (1997). The corresponding wind luminosity is $L_w \approx 500 L_\odot$.

The age of the source can be estimated in two ways. First, using the mean density, the dynamical time is $\tau_{dyn} = 1/\sqrt{G\rho} \approx 3 \times 10^{12}$ s. Second, using the force exerted by the hot, X-ray emitting gas; as just noted, the latter has a much lower density than the absorbing gas, but a similar pressure. The outward acceleration is $P_x/\Sigma \approx 10^{-7}$ cm s^{-2} . The dynamical time is then $\tau_{dyn} \approx 2 \times 10^{12}$ s, roughly the same as the estimate based on the self-gravity of the cold gas.

Assuming that the stellar wind is trapped in a Castor style bubble, the energy in the shocked gas is $E = \frac{5}{11} L_w \tau \approx 4 \times 10^{48}$ erg s^{-1} , and the pressure $P = 2 \times 10^{-5}$ dynes cm^{-2} , two orders of magnitude higher than observed (and with an associated X-ray luminosity four orders of magnitude too high). Since this pressure is so much higher than the dynamical pressure, and the sound crossing time of the hot gas so much smaller (by a factor of about 1000), the simplest interpretation is simply that the shocked stellar wind gas escapes, as in Carina. The radio images of the G sources in Figure 2 of De Pree et al. (2000) show a very incomplete ring, strengthening the argument for rapid escape.

The second case is the ultracompact H II region G 5.97 -1.17 associated with the Hourglass nebulae in M8. It is believed to be powered by the O7 V star Herschel 36; using values for \dot{M}_w from Repolust et al (2004) (not allowing for a clumped wind), we estimate

$L_w = 2 \times 10^{36}$ erg s⁻¹, while Rauw et al. (2002) use a wind luminosity a factor of 3 smaller. They estimate a dynamical age of 2×10^4 yr based on the size of the Hourglass (they use $R = 0.2$ pc) and the observed expansion velocity of 10 km s⁻¹ (Chakraborty & Anandarao 1997, 1999). Using their values for L_2 , τ_{dyn} , and R_b , we find a predicted hot gas pressure of $P = 4 \times 10^{-7}$ and $n_x \approx 200$ cm⁻³. The predicted $L_x = 7 \times 10^{35}$ erg s⁻¹, larger than that observed by a factor of 1000. Using the full Castor et al. model, Rauw et al. (2002) note that the predicted bubble radius is larger than that observed (but only by a factor of 2) and that the predicted X-ray flux is $L_x \approx 10^{35}$ erg s⁻¹. This smaller than our prediction by a factor of 7, consistent with their use of the (two times too large) Castor et al. radius. Their predicted X-ray flux is still larger than observed by a factor of 175.

Radio observations by Turner et al. (1974) find a radius $r \sim 0.1$ pc (half that suggested by Rauw et al.) and a flux at 11 cm of 0.54 Jansky. The H II gas pressure is 1.5×10^{-9} dynes cm⁻² from the observed radio flux, and 1.5×10^{-8} dynes cm⁻² using Q for an O 7 V star. This should be compared to the pressure of the X-ray emitting gas $P_x = 8 \times 10^{-9}$ dynes cm⁻², and to the radiation pressure $L/4\pi r^2 c = 1.6 \times 10^{-8}$ dynes cm⁻². All these pressures are at least a factor 10 below the pressure found under the assumption that the wind luminosity is trapped in the bubble. We conclude that, as for G_x, the most likely explanation of the low observed X-ray flux and the small bubble radius is that the shocked stellar gas simply escapes from the bubble interior.

7. CONCLUSIONS

We use both the Castor et al. theory and the Chevalier and Clegg theory for bubble evolution around massive star clusters to try to understand observations of Milky Way and LMC bubbles. The Castor theory over-predicts X-ray luminosity in the Carina bubble by a factor of 60 and expands too fast by a factor of 4. In contrast, the Chevalier and Clegg model under predicts the X-ray luminosity by a factor of 20; since it is a steady state it has no expansion time.

These results suggest there is a partially confined hot, homogeneous interior but there are also holes in the shell through which the hot gas escapes like a free flowing wind. We constructed a model in which the confining shell covered only a fraction C_f of the sky as seen from the cluster, and allowed hot wind gas to escape at its sound speed from the uncovered portion of the shell. As an example one model consistent with observations of Carina is an isothermal sphere GMC model with $R_G = 60$ pc, $\alpha = 0.2$, and $C_f = 0.5$, $R_b = 16.5$ pc, $L_x = 1.2 \times 10^{34}$ erg s⁻¹, and $P_b = 1.1 \times 10^{-10}$ dynes cm⁻². This compromise is the best way to fit the many observations of the Carina nebula and is likely the best solution for all bubbles. Our models suggest that the exact size, distribution and evolution of holes does

not matter much, it is the weighted average of the fraction of total area that matters.

The bottom line is that the dynamics of X-ray bubbles are not strongly affected by the presence of luminous stellar winds; rather, they are controlled by a combination of the self-gravity of the surrounding GMC gas, radiation pressure, and H II gas pressure. This conclusion is in contrast to that of Castor et al. (1975) and Shull (1980), but in agreement with McKee, Van Buren, & Lazareff (1984). We argue that the X-ray fluxes of the bubbles are *always* below those predicted by the Castor et al. picture, properly interpreted, i.e., using the observed rather than predicted bubble radii. As noted by Dorland, Montmerle, & Doom (1986); Dorland & Montmerle (1987), the X-ray observations show that the pressure in the hot gas is well below that predicted by Castor et al. (1975); unlike Dorland, Montmerle, & Doom (1986); Dorland & Montmerle (1987) and McKee, Van Buren, & Lazareff (1984), we argue that this is a result of leakage of hot gas from the bubble, rather than leakage of energy in the form of radiation.

The results of the models in this paper are dependent upon the ISM model used, both the run of mean density, and the fluctuations in the surface density in different directions from the bubble center. According to both simulations and observations, the latter is distributed log-normally, meaning that in many directions the surface density will be far below the mean surface density. We suggest that hot gas escapes along these directions, which in our simplified models we treat as holes in the bubble wall.

Full hydrodynamical models are needed to check that the semi-analytical solutions shown in this paper are correct and to understand both the early evolution of bubbles and the development of holes in the shell.

We would like to thank C. De Pree for allowing us to use Fig. 13. This research has made use of the SIMBAD database, operated at CDS, Strasbourg, France, and of NASA’s Astrophysics Data System. This work was supported by NSERC of Canada. N.M. is supported in part by the Canada Research Chair program, and by NSERC of Canada.

A. CHEVALIER & CLEGG BUBBLES

Chevalier & Clegg assume a spherically symmetric wind with mass input \dot{M}_w and energy input $\dot{E} = L_w$. For a smooth transition from subsonic flow at the centre to supersonic flow at large distances the Mach number must equal one at some radius, which Chevalier & Clegg take to be $r = R_{cl}$.

The flow is described by

$$\frac{1}{r^2} \frac{d}{dr} (\rho u r^2) = \phi, \tag{A1}$$

$$\rho u \frac{du}{dr} = -\frac{dP}{dr} - \phi u, \quad (\text{A2})$$

$$\frac{1}{r^2} \frac{d}{dr} \left[\rho u r^2 \left(\frac{1}{2} u^2 + \frac{5P}{2\rho} \right) \right] = \Phi, \quad (\text{A3})$$

where u is the wind velocity, r is the radial co-ordinate, ρ is the density, P is the pressure, and γ , the adiabatic index, = 5/3 through this paper. For $r < R_{cl}$, $\phi = \dot{M}_w/V$, $\Phi = \dot{E}/V$, $V = 4\pi R_{cl}^3/3$; for $r > R_{cl}$, $\phi = \Phi = 0$. Equations (A1)-(A3) have the solution

$$\left(\frac{5 + 1/\mathcal{M}^2}{6} \right)^{\left(-\frac{9}{14}\right)} \left(\frac{1 + 3/\mathcal{M}^2}{4} \right)^{\left(\frac{1}{7}\right)} = \frac{r}{R_{cl}}, \quad (\text{A4})$$

for $r < R_{cl}$, and

$$\mathcal{M}^3 \left(\frac{1 + 3/\mathcal{M}^2}{4} \right)^2 = \left(\frac{r}{R_{cl}} \right)^2, \quad (\text{A5})$$

for $r > R_{cl}$, where \mathcal{M} is the Mach number.

The flow can be integrated in two sections, $r < R_{cl}$ and $r > R_{cl}$ using the outer boundary conditions of the first as the inner boundary of the second. Thus, it is possible to follow the evolution of the wind and numerically integrate the expected X-ray luminosity from the cluster edge out to arbitrarily large distances..

Initially a small radius ($r \ll R_{cl}$) and small initial mach number, \mathcal{M}_0 are assumed. The true Mach number is then found iteratively to 10 decimal places for that radius

$$\mathcal{M}_{i+1} = \left[6 \left(\frac{1 + 3/\mathcal{M}^2}{4} \right)^{\frac{2}{9}} \left(\frac{r}{R_{cl}} \right)^{-\frac{11}{9}} - 5 \right]^{-0.5}. \quad (\text{A6})$$

The calculated Mach number was then combined with the observed mass loss rate and stellar wind luminosity for Tr 16 (Table 1) to find the initial conditions (from Chevalier & Clegg (1985))

$$\begin{aligned} \rho &= 0.296 \dot{M}_w^{1.5} L_w^{-0.5} R_{cl}^{-2}, \\ n &= \frac{\rho}{\mu}, \\ P &= 0.118 \dot{M}_w^{0.5} L_w^{0.5} R_{cl}^{-2}, \\ T &= \frac{P}{nk_b}, \\ c_s &= \sqrt{\frac{5P}{3\rho}}, \\ u &= \mathcal{M}c_s. \end{aligned}$$

From these initial conditions equations (A1)-(A3) can be integrated to the cluster radius. The integration continues with the evolution equations (without the source terms outside the cluster) and the appropriate Mach number iteration,

$$\mathcal{M}_{i+1} = \left(\frac{r}{R_{cl}} \right)^{\frac{2}{3}} \left(\frac{4}{1 + 3/\mathcal{M}_i} \right)^{\frac{1}{6}}. \quad (\text{A7})$$

B. CASTOR et al. BUBBLES

For a bubble in the snow plough stage, R_b is large enough that the flow from c to b can be considered stationary and plane parallel. Weaver et al. (1977) considered the effects of relaxing this assumption and found the results are only changed by $\leq 10\%$, much less than the observational errors for, e.g., the bubble radius in Carina. For a stationary plane parallel flow at constant pressure (Penston & Brown 1970)

$$\rho v \frac{dH}{dz} = \frac{d}{dz} \left[K(T) \frac{dT}{dz} \right] - \rho \Lambda(T), \quad (\text{B1})$$

where T is temperature, $z = R_b - r$, $\rho v = \dot{M}_b / 4\pi R_b^2$, M_b is the mass in region b, $H = 5k_b T / 2\mu$ the specific enthalpy, $K(T) = CT^{5/2}$ is the thermal conductivity, and $C = 1.2 \times 10^{-6} \text{ erg cm}^{-1} \text{ s}^{-1} \text{ K}^{7/2}$ (Spitzer 1962). Integrating equation(B1) from the b-c boundary: $z = 0$, $T \sim 0$ to the centre: $z = R_b$, $T = T_b$ gives the mass evaporating from c to b as

$$\dot{M}_b = \frac{16\pi}{25} \frac{\mu}{k_b} K(T) R_b. \quad (\text{B2})$$

To get this solution we have assumed the cooling term, $\rho \Lambda(T)$ is negligible in the transition zone between b and c.

Energy is constantly added into region b by the stellar winds with the total luminosity L_w and the dominant energy loss is through the expansion of the bubble. The energy in region b obeys

$$\dot{E}_b = L_w - 4\pi R_b^2 P_b \dot{R}_b, \quad (\text{B3})$$

where P_b is the pressure in region b and

$$\frac{4}{3} \pi R_b^3 P_b = \frac{2}{3} E_b. \quad (\text{B4})$$

When considering radiative losses from region b it is necessary to follow the evolution of region a (the hypersonic stellar wind region) as eventually region b will cool enough to

collapse. Therefore, the equations need to be altered to account for the fact that the size of region a is not negligible. In that case, the energy in region b is given by

$$E_b = 2\pi P_b(R_b^3 - R_a^3), \quad (\text{B5})$$

where R_a is the radius of region a. R_a can be calculated from pressure balance at R_a . The pressure from region b on a shell at R_a is

$$P_b = \frac{1}{2\pi} \frac{E_b}{R_b^3 - R_a^3}. \quad (\text{B6})$$

The stellar wind luminosity is $L_w = \dot{M}_w v_w^2 / 2$ so the rate of momentum deposition by the stellar wind is

$$\dot{M}_w v_w = \frac{2L_w}{v_w}. \quad (\text{B7})$$

This then gives a pressure at radius R_a of

$$P_w = \frac{2L_w}{v_w} \frac{1}{4\pi R_a^2}. \quad (\text{B8})$$

Setting these pressures equal gives

$$R_a = \left[\frac{L_w}{v_w E_b} (R_b^3 - R_a^3) \right]^{1/2}. \quad (\text{B9})$$

Radiative losses within region b can be calculated by reference to the cooling functions in Sutherland & Dopita (1993)

$$L_b \approx n_b^2 \frac{4}{3} \pi (R_b^3 - R_a^3) \Lambda(T). \quad (\text{B10})$$

Including radiative losses into the Castor et al. evolution equations results in the following closed set of evolution equations

$$\frac{d\mathcal{P}_c}{dt} = 4\pi R_b^2 P_b, \quad (\text{B11})$$

$$\frac{dR_b}{dt} = \frac{\mathcal{P}_c}{M_c}, \quad (\text{B12})$$

$$\frac{dM_b}{dt} = C_1 T_b^{5/2} R_b^2 (R_b - R_a)^{-1} - 10^{-5} \frac{\mu}{k_b} L_b, \quad (\text{B13})$$

$$\frac{dE_b}{dt} = L_w - 4\pi R_b^2 P_b \frac{dR_b}{dt} - L_b, \quad (\text{B14})$$

where \mathcal{P}_c is the momentum of the shell and $C_1 = 4.13 \times 10^{-14}$ cgs.

The initial conditions of the bubble are taken from Weaver et al. (1977) at time $t_0 = 10^3$ years:

$$E_b = \frac{5}{11} L_w t_0, \quad (\text{B15})$$

$$R_b = \left(\frac{125}{154\pi} \frac{L_w}{\rho_0} \right)^{1/5} t_0^{3/5}, \quad (\text{B16})$$

$$v_c = \frac{3}{5} \frac{R_b}{t_0}, \quad (\text{B17})$$

$$V_b = \frac{4}{3} \pi R_b^3, \quad (\text{B18})$$

$$P_b = \frac{E_b}{V_b}, \quad (\text{B19})$$

$$M_b = \frac{28}{205} \times 1.646^{5/2} \times V_b \frac{\mu}{k_b} \left(\frac{t_0 C}{R_b^2} \right)^{2/7} P_b^{5/7}, \quad (\text{B20})$$

$$\rho_b = \frac{M_b}{V_b}, \quad (\text{B21})$$

$$n_b = \frac{\rho_b}{\mu}, \quad (\text{B22})$$

$$T_b = \frac{P_b}{n_b k_b}. \quad (\text{B23})$$

These give initial conditions close enough to the true values that the numerical solution settles down by the cluster boundary and is a valid solution for $R_b > R_{\text{cl}}$.

Initially the parameters were set up to match those used in Weaver et al. (1977) and results compared to Figure 6 of that paper as a check of our code. Once the code was tested parameters for Tr 16 could be used (from Table 1).

REFERENCES

- Allen, D. A., & Hillier, D. J. 1993, Proceedings of the Astronomical Society of Australia, 10, 338
- Bouret, J.C., Lanz, T., and Hillier, D.J. 2005, A&A, 438, 301
- Bressan, A., Fagotto, F., Bertelli, G., & Chiosi, C. 1993, A&AS, 100, 647
- Cantó, J., Raga, A., & Rodríguez, L. 2000, ApJ 536, 896
- Castor, J., McCray, R., and Weaver, R. 1975, ApJ, 200, L107

- Chakraborty, A. & Anandarao, B. G. 1997, *AJ*, 114, 1576
- Chakraborty, A. & Anandarao, B. G. 1999, *A&A*, 346, 947
- Chevalier, R. A. & Clegg, A. W. 1985, *Nature*, 317, 44
- Chu, Y.-H., & Mac Low, M.-M., 1990, *ApJ*, 365, 510
- Chu, Y.-H., Chang, H.-W., Su, Y.-L., & Mac Low, M.-M., 1995, *ApJ*, 450, 157
- Cowie, L.L. & McKee, C.F. 1977, *ApJ*, 211, 135
- De Pree, C. G., Mehringer, D. M., & Goss, W. M. 1997, *ApJ*, 482, 307
- De Pree, C. G., Wilner, D. J., Goss, W. M., Welch, W. J., & McGrath, E. 2000, *ApJ*, 540, 308
- De Pree, C. G., Wilner, D. J., Deblasio, J., Mercer, A. J., & Davis, L. E. 2005, *ApJ*, 624, L101
- Dopita, M. A. et al., 2005, *ApJ*, 619, 755
- Dorland, H., Montmerle, T., & Doom, C. 1986, *A&A*, 160, 1
- Dorland, H. & Montmerle, T. 1987, *A&A*, 177, 243
- Dunne, B. C. et al. 2003, *ApJ*, 590, 306
- Evans, C. J., Crowther, P. A., Fullerton, A. W., and Hillier, D. J. 2004, *ApJ*, 610, 1021
- Flaccomio, E. 2005, *Massive Star Birth: A Crossroads of Astrophysics*, Proceedings IAU Symposium No. 227, ed. R. Cesaroni, M. Felli, E. Churchwell and C. M. Walmsley
- Fullerton, A.W., Massa, D.L., and Prinja, R.K. 2006, *ApJ*, 637, 1025
- Gilman, R.C. 1974, *ApJS*, 28, 397
- Goodman, A. A., Pineda, J. E., & Schnee, S. L. 2008, *ArXiv Astrophysics e-prints*, arXiv:astro-ph/0806.3441
- Grabelsky, D. A., Cohen, R. S., Bronfman, L. & Thaddeus, P. 1988, *ApJ*, 331, 181
- Hamaguchi, K. et al. 2007, *PASJ*, 59, S151
- Hamaguchi, K. et al. 2007b, *PThPS*, 169, 174

- Huchtmeier, W.K. and Day, G.A. 1975, *A&A*, 41, 153
- Kennicutt, R. C. 1989, *ApJ*, 344, 685
- Kennicutt, R. C. 1998, *ApJ*, 498, 541
- Laor, A., and Draine, B. T. 1993, *ApJ*, 402, 441
- Lopez, J.A., and Meaburn, J. 1984, *Rev. Mexicana Astron. Astrofis.*, 9, 119
- Lucke, P. B., & Hodge, P. W. 1970, *AJ*, 75, 171
- McGee, R. X., Brooks, J. W., & Batchelor, R. A. 1972, *Aust. J. Phys.*, 25, 58
- McKee, C. F., Van Buren, D., & Lazareff, B. 1984, *ApJ*, 278, 115
- Murray, N., Quataert, E., and Thompson, T.A. 2008, in prep.
- Oey, M. S. 1996, *ApJ*, 467, 666
- Ostriker, E. C., Stone, J. M., & Gammie, C. F. 2001, *ApJ*, 546, 980
- Passot, T., & Vazquez-Semadeni, E. 1998, *Phys. Rev. E*, 58, 4501
- Penston, M.V. and Brown, F.E. 1970, *MNRAS*, 150, 373
- Povich, M.S., Benjamin, R.A., Whitney, B.A., Babler, B.L., Indebetouw, R., Meade, M.R., & Churchwell, E. 2008, *ApJ*, 689, 242
- Press, W.H, Teukolsky, S.A., Vetterling, W.T., Flannery, B.P. 1996, *Numerical Recipes in Fortran 90, Second Edition* (Cambridge University Press)
- Puls, J., et al. 2006 *A&A*, 454, 625
- Rauw, G., Nazé, Y., Gosset, E., Stevens, I. R., Blomme, R., Corcoran, M. F., Pittard, J. M., & Runacres, M. C. 2002, *A&A*, 395, 499
- Repolust, T., Puls, J., and Herrero, A. 2004, *A&A*, 415, 349
- Retallack, D.S. 1983, *MNRAS*, 204, 669
- Sanchawala, K., Chen, W.P., Lee, H.T., Chu, Y.H., Nakajima, Y., Tamura, M., Baba, D., and Sato, S. 2007, *ApJ*, 656, 462
- Scoville, N. Z., & Kwan, J. 1976, *ApJ*, 206, 718

- Seward, F.D., Forman, W.R., Giacconi, R., Griffiths, R.E., Harnden, Jr., F.R., Jones, C., and Pye, J. P. 1979, *ApJ*, 234, L55
- Schull, J. M. 1980, *ApJ*, 238, 860
- Smith, B. J., Struck, C., & Nowak, M. A. 2005, *AJ*, 129, 1350
- Smith, N. 2006a, *MNRAS*, 367, 763
- Smith, N. 2006b, *ApJ*, 644, 1151
- Smith, N. & Brooks, K. J. 2007a, *MNRAS*, 379, 1279
- Smith, N. and Brooks, K.J. 2007b, in *Handbook of Star Forming Regions*, ed. B. Reipurth, in press
- Spitzer, L., Jr. 1962, *Physics of Fully Ionised Gases* (New York: Interscience)
- Stevens, I.R. and Hartwell, J.M. 2003, *MNRAS*, 339, 280
- Sutherland, R.S. and Dopita, M.A. 1993 *ApJS*, 88, 253
- Townsley, L. K., Feigelson, E. D., Montmerle, T., Broos, P. S., Chu, Y.-H., & Garmire, G. P. 2003, *ApJ*, 593, 874
- Townsley, L. K., Broos, P. S., Feigelson, E. D., Brandl, B. R., Chu, Y.-H., Garmire, G. P., & Pavlov, G. G. 2006, *AJ*, 131, 2140
- Tsujimoto, M., Hosokawa, T., Feigelson, E. D., Getman, K. V., & Broos, P. S. 2006, *ApJ*, 653, 409
- Turner, B. E., Balcik, B., Cudaback, D. D., & Heiles, C. 1974, *ApJ*, 194, 279
- Walborn, N. R., & Hesser, J. E. 1975, *ApJ*, 199, 535
- Walborn, N. R., & Hesser, J. E. 1982, *ApJ*, 252, 156
- Wang, Q., & Helfand, D. J. 1991, *ApJ*, 373, 497
- Weaver, R., McCray, R., Castor, J., Sharpir, P., and Moore, R. 1977, *ApJ*, 218, 377
- Whiteoak, J.B.Z. 1994, *ApJ*, 429, 225
- Wong, T., et al., 2008 *MNRAS*, 386, 1069

Yonekura, Y., Asayama, S., Kimura, K., Ogawa, H., Kanai, Y., Yamaguchi, N., Barnes, P. J., & Fukui, Y. 2005, *ApJ*, 634, 476

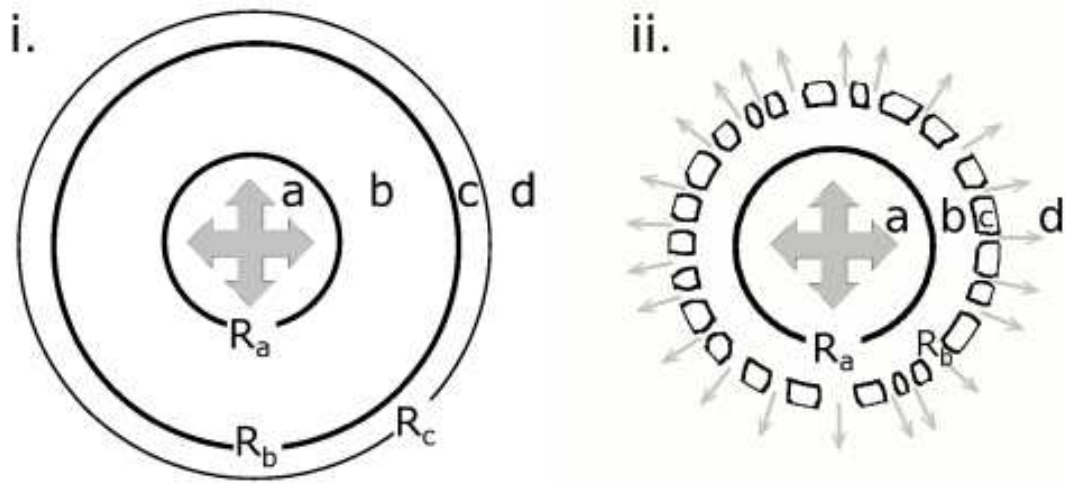


Fig. 1.— Cartoons of the Castor et al. bubble (i.) and the modified Castor et al. bubble (ii.). The Castor et al. bubbles have a four zone structure. Zone a is hypersonic stellar wind; zone b is shocked stellar wind and evaporated material from the shell; zone c is the bubble shell; and zone d is the ambient ISM. ii. - The structure of the modified Castor et al. bubble, showing leaking from the shell. Note the larger size of region a, smaller size of region b and material escaping into region d.

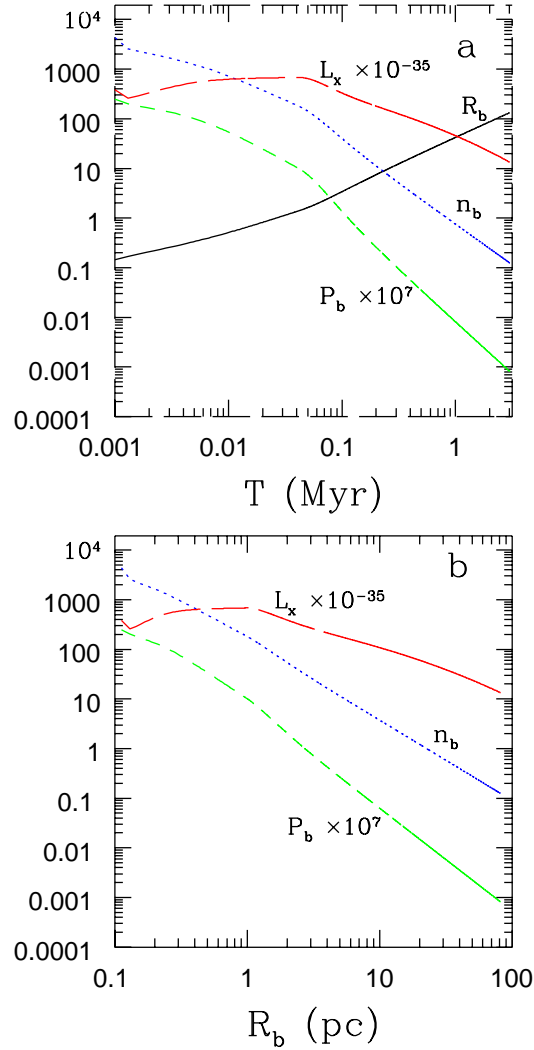


Fig. 2.— Plots of the basic Castor et al. (1975) model evolution against time (a) and R_b (b) for Tr 16. These plots show how pressure, number density and total X-ray luminosity change through the evolution of the bubble. Pressure and X-ray luminosity have been scaled to fit on the graphs.

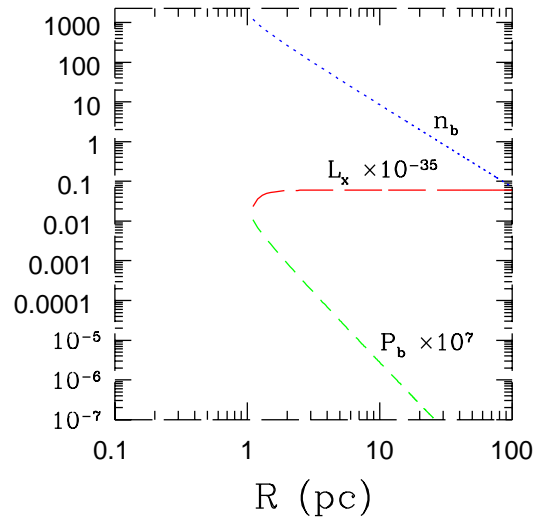


Fig. 3.— Plot of the steady state Chevalier & Clegg (1985) model for Tr 16. The number density, pressure and X-ray luminosity against radius are plotted. Pressure and X-ray luminosity have been scaled to fit on the graphs. Note that we plot the *cumulative* X-ray luminosity as a function of radius.

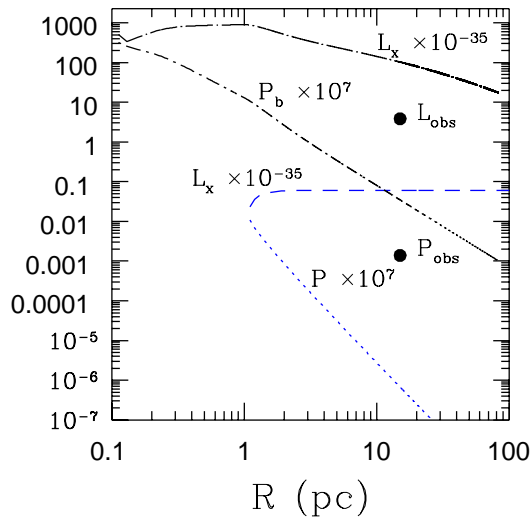


Fig. 4.— Plot of the scaled X-ray luminosity and pressure calculated as a function of radius for the two classes of (unmodified) models for Tr 16, as discussed in §4.1. The Castor model is plotted as a function of bubble size whereas the Chevalier model is plotted as a cumulative function of radius (due to its steady state nature). The upper L_x and P lines are for the Castor model and the lower lines for the Chevalier model. The two dots show the observed pressure (lower) and X-ray luminosity (upper). In the Castor et al. model the pressure is roughly constant for $r < R_b$, but this constant pressure is a function of the bubble radius, as shown. In the Chevalier & Clegg model there is no bubble, but pressure decreases with increasing radius.

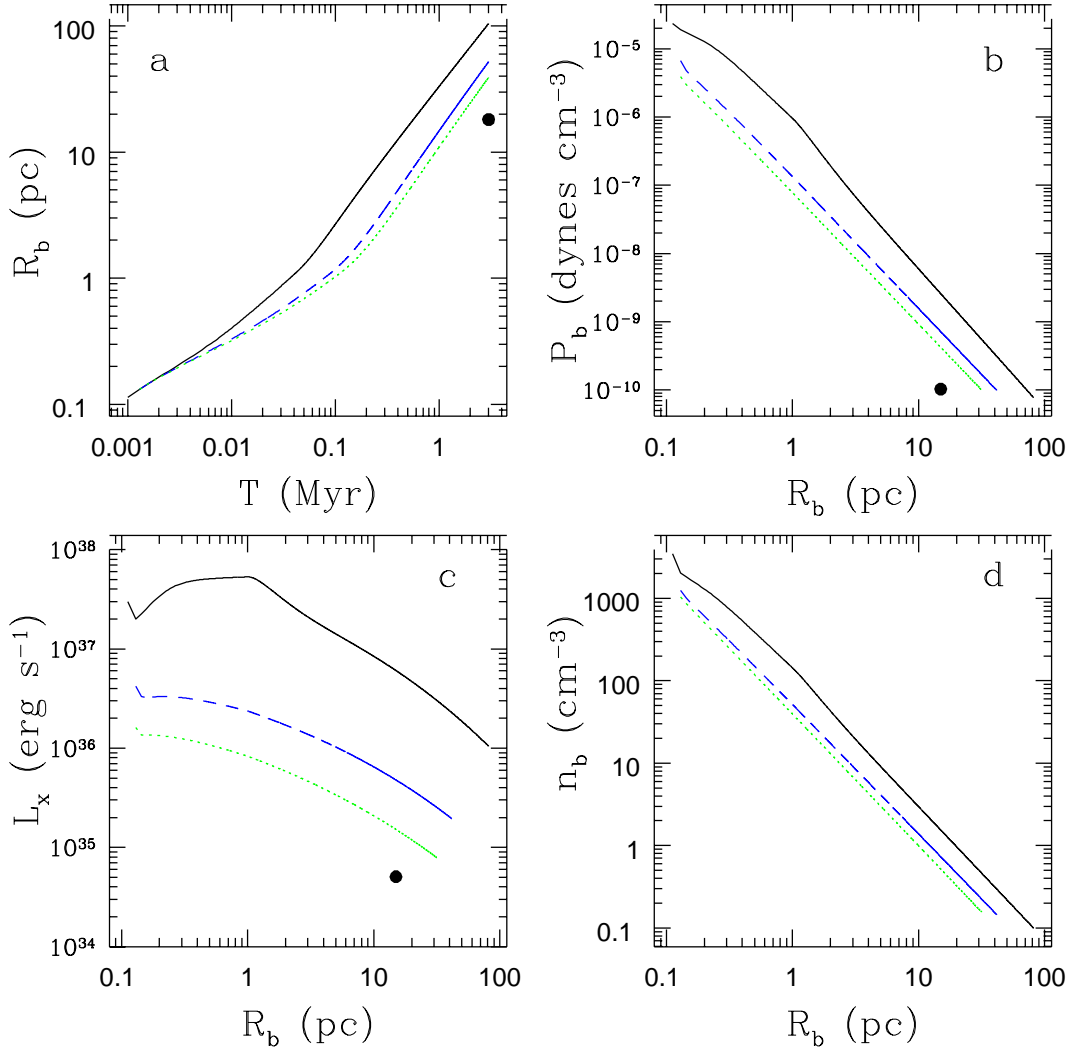


Fig. 5.— Graphs for three modified Castor simulations with $C_f = 1$ (solid), $C_f = 0.65$ (dashed), and $C_f = 0.3$ (dotted). (a) radius versus time, (b) pressure versus radius, (c) X-ray luminosity versus radius, and (d) number density inside the bubble versus radius. Observed results are shown as a black dot. See the discussion in §4.2.

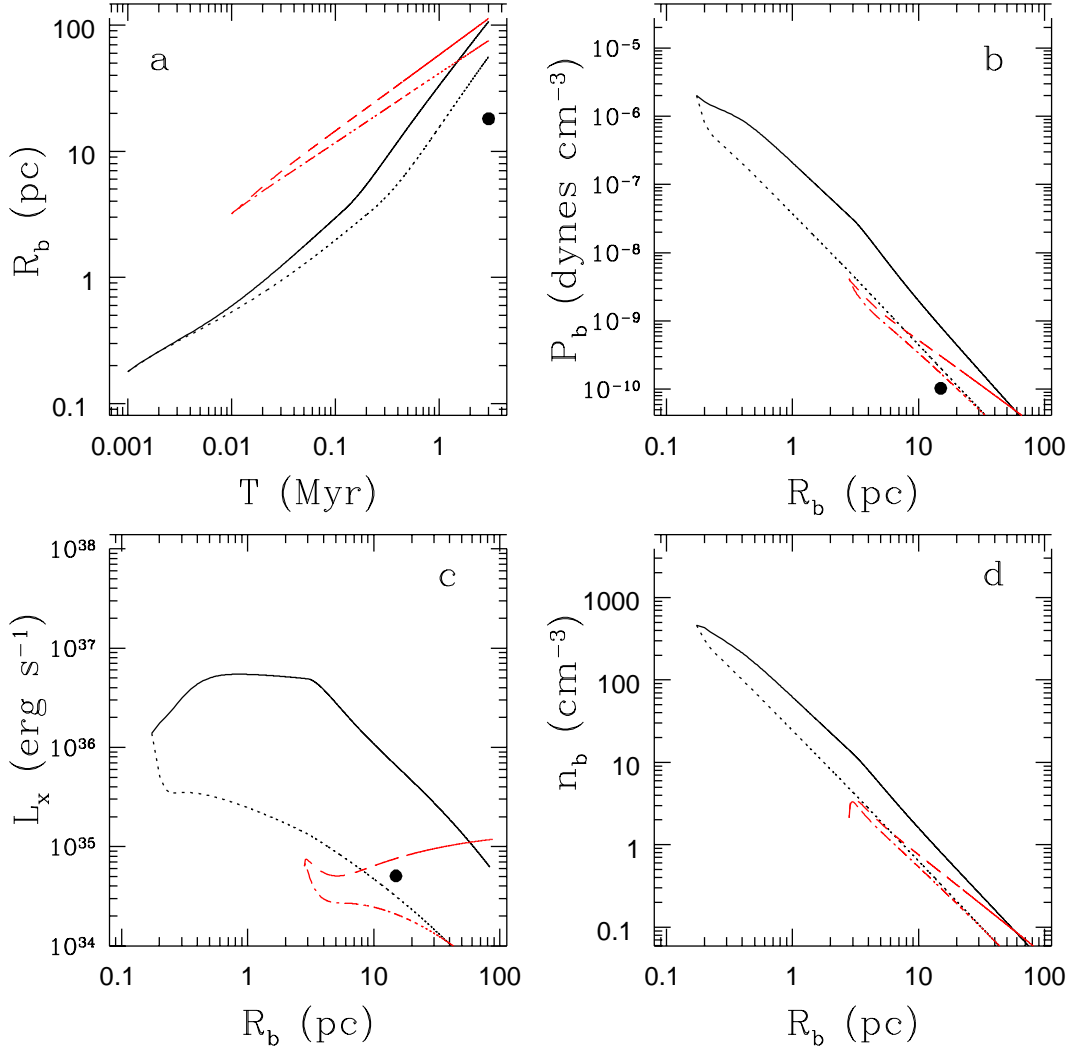


Fig. 6.— Graphs showing the details of modified Castor simulations with different ISM models and different shell cover factors C_f . All runs have $R_{cl} = 3$ pc, $R_G = 73.86$ pc and $\alpha = 1/3$. (a) is R_b versus time, (b) pressure versus R_b , (c) X-ray luminosity versus R_b , and (d) n_b versus R_b . The solid line is for an isothermal GMC, with $C_f = 1$, the dotted line is an isothermal GMC with $C_f = 0.5$, the dashed line has constant ISM density with $C_f = 1$, and the dash-dotted line has constant ISM density with $C_f = 0.5$. Note that (b) and (c) are plotted against radius so although some models do fit the observed quantities at that radius they do so after too short a time.

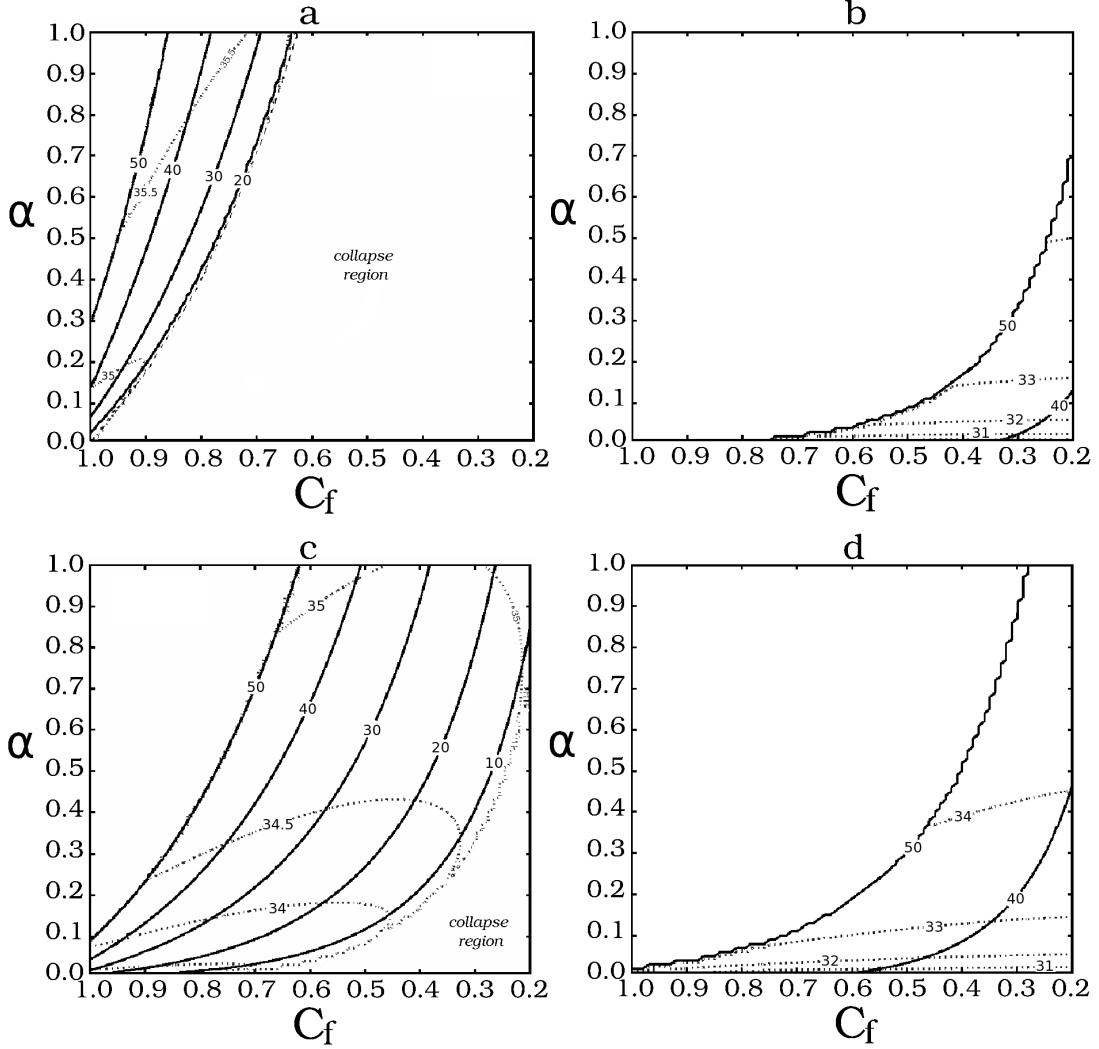


Fig. 7.— Parameter study results for varying α and C_f for either an isothermal sphere ISM and for $R_G = 24$ pc (a) or $R_G = 60$ pc (c), or for a constant density ISM for $R_G = 24$ (b) or $R_G = 60$ pc (d) modified Castor models at 3Myrs. The contours show the X-ray luminosity (dotted) and the radius (solid). Gray dashed lines show the boundary of the collapse region. X-ray luminosity is in logarithmic contours in intervals of $\times 10$ erg s^{-1} for the homogeneous models and $\times 10^{0.5}$ erg s^{-1} for the isothermal models. Radius contours are linear in intervals of 10 parsecs. The observed properties of Carina are $13 < R_b < 20$ pc and $L_x = 4.8 \times 10^{34}$ erg s^{-1} . For the isothermal ISM model there are regions of the parameter space where the shell collapses inwards in the simulations. This is due to the swept up mass being so large the gravitational force is larger than the sum of the gas pressure force and radiation pressure force.

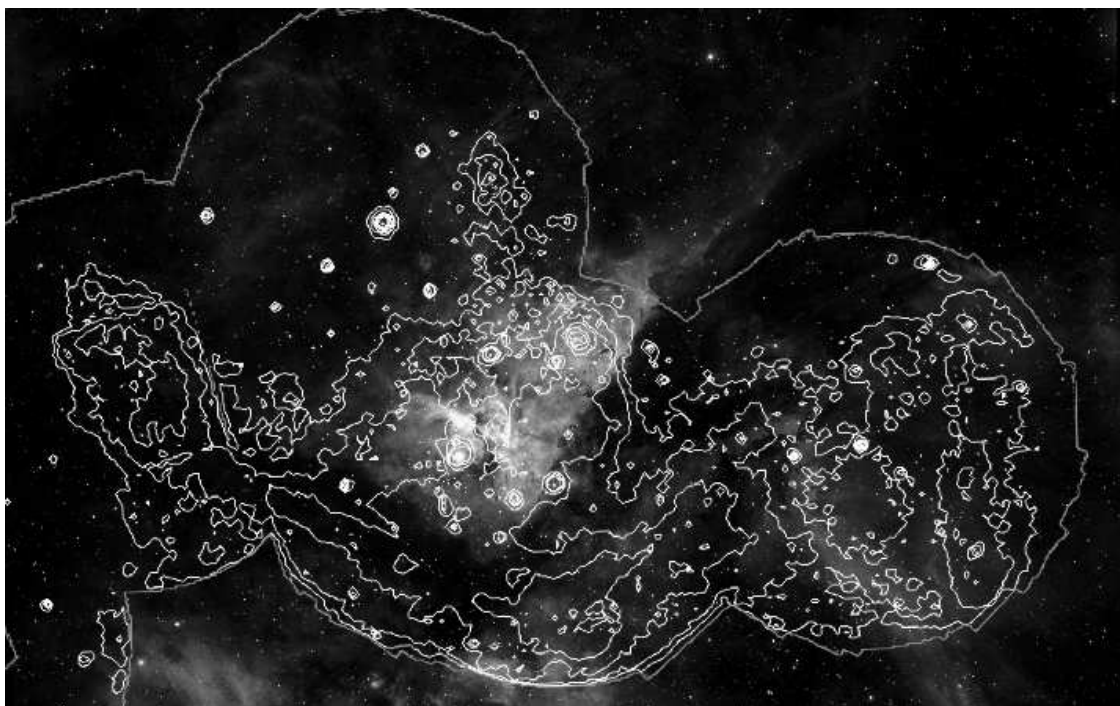


Fig. 8.— Image of the Carina nebula in visual (Smith & Brooks 2007a) and X-ray contours (Hamaguchi et al. 2007a). The visual image is a combination of H II, O IV and S II and the X-ray image is between 0.7 keV and 1.3 keV. The green outline shows the edge of the X-ray image. See the electronic edition of the Journal for a color version of this Figure.

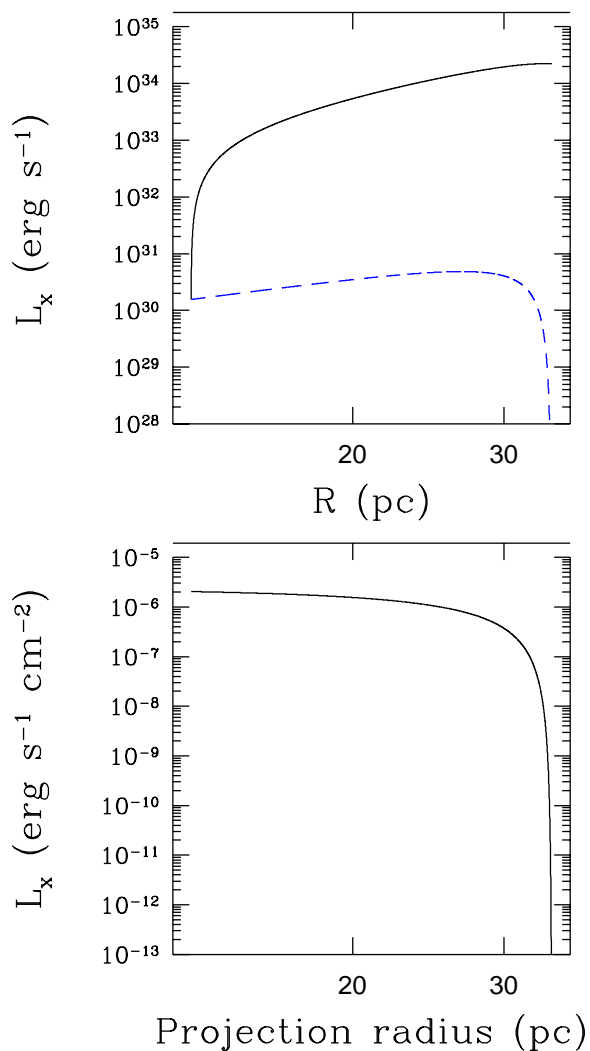


Fig. 9.— Graphs of a modified Castor model showing (a) the cumulative X-ray luminosity (solid) and X-ray profile (dashed) with 3D radius; (b) shows the X-ray profile with projected radius (z); we expect an almost flat X-ray profile with a sharp cutoff at the bubble edge. This model is for $\alpha = 1/3$, $C_f = 0.5$, isothermal sphere ISM model with $R_G = 60$ pc.

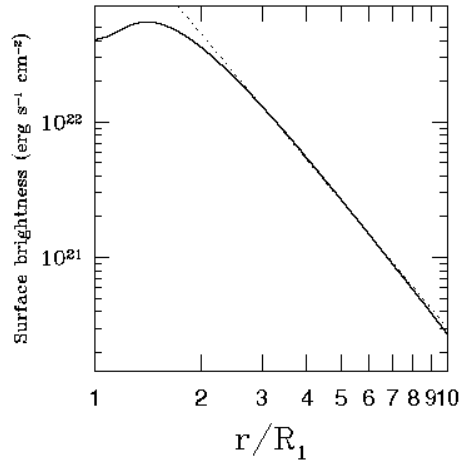


Fig. 10.— The X-ray emission profile against r/R_1 for $T_f = 10^6$ and $R_1 = 1$ pc for an evaporating globule (solid line) showing a fairly sharply defined X-ray halo. The dotted line shows a gradient of -3.

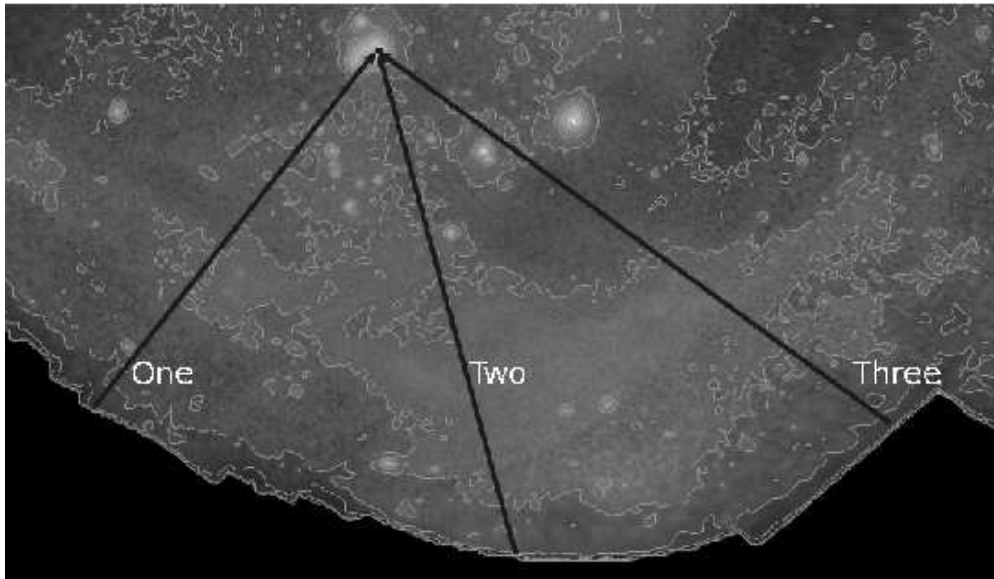


Fig. 11.— XMM image of the southern part of the Carina Nebula between 700 eV and 1300 eV with contours. η Carina can be seen along the top (with all three profile lines pointing at it). Thick lines are the profile lines used in Fig. 12.

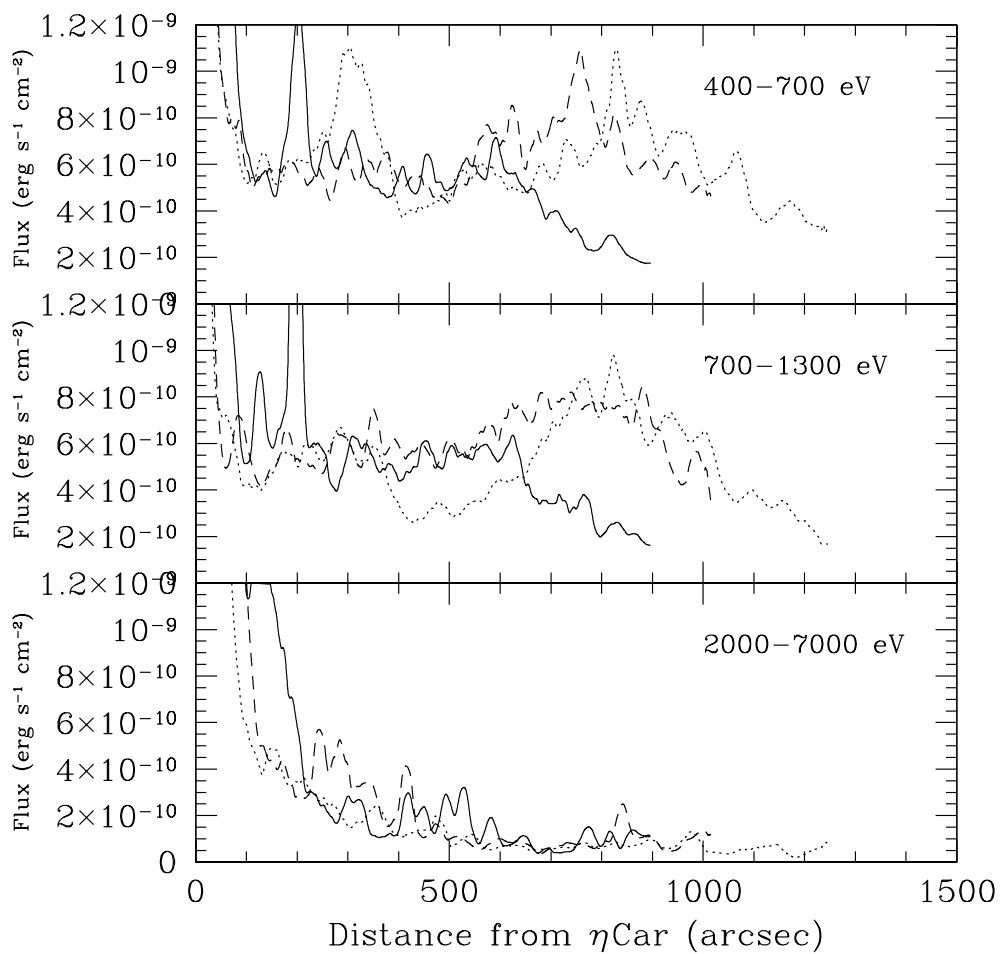


Fig. 12.— Surface brightness along the lines in Fig. 11 for the three different XMM bands. The solid line is for profile one, the dashed line for profile two and dotted line for profile three. Surface brightness is given in $\text{erg cm}^{-2} \text{s}^{-1}$, with an assumed $N_H = 1.8 \times 10^{21} \text{ cm}^{-2}$ (Hamaguchi et al. 2007a); projected distances from η Carina are given in arcseconds. Recall that at a distance of 2.3 kpc, 1000 arcseconds is about 11 pc.

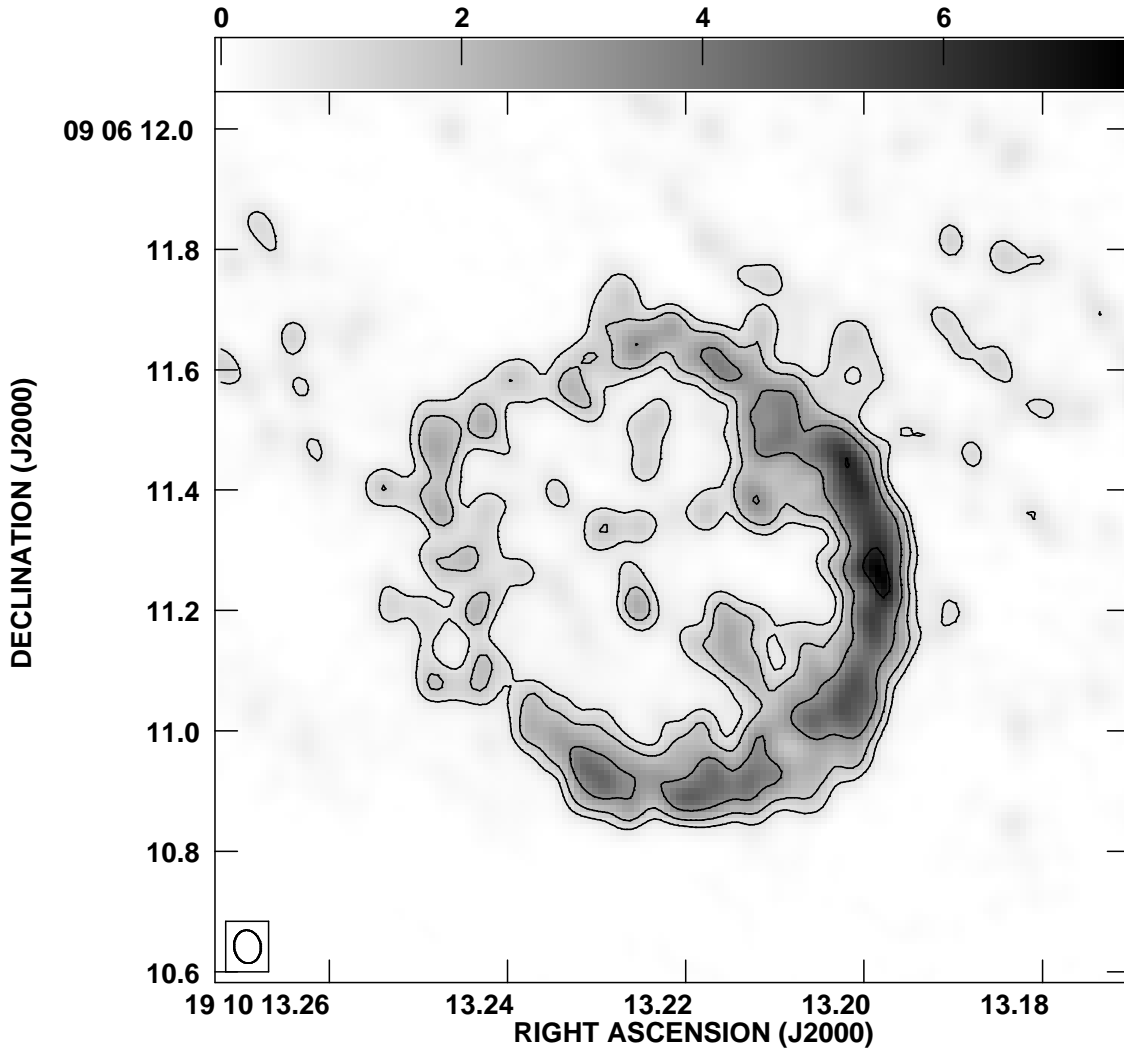


Fig. 13.— VLA 7mm observation of W49A/D from De Pree et al. (2005). Beam size shown lower left is about 500 AU. The shell has a radius of ~ 0.03 pc and the column density through the shell is significantly variable.

Number of stars \geq B2	72
Total bolometric luminosity	$1.7 \times 10^7 L_{\odot}$
Total ionizing flux (Q)	$5.9 \times 10^{50} \text{ s}^{-1}$
Total mass loss rate \dot{M}_w	$1.1 \times 10^{-3} M_{\odot}/\text{year}$
Total stellar wind luminosity	$6.7 \times 10^4 L_{\odot}$

Table 1: Properties of Tr 16 in the Carina Nebula using all stars of spectral type B2 or earlier assuming standard mass loss rates (Repolust et al 2004). From Smith (2006a).

T/K	$L_d / \text{erg s}^{-1}$	Q_e	M_d/M_{\odot}
35	2.93×10^{40}	8.72×10^{-5}	6 610
80	1.19×10^{40}	4.71×10^{-4}	18.2
220	4.24×10^{39}	3.72×10^{-3}	0.014

Table 2: Dust masses of the three components seen in Smith & Brooks (2007a) with better dust modeling, compared to Smith & Brooks (2007a) total dust mass of $9.6 \times 10^3 M_{\odot}$